RIVISTA DEL NUOVO CIMENTO Vol. 32, N. 12 2009
DOI 10.1393/ncr/i2010-10050-5

High-energy neutrino astronomy

P. Sapienza and G. Riccobene

Laboratori Nazionali del Sud, Istituto Nazionale di Fisica Nucleare
Via S. Sofia 62, I-95123, Catania, Italy

(ricevuto il 2 Novembre 2009)

Summary. — The field of astroparticle physics entered in a flourishing period thanks to the operation of several experiments that lead to the discovery and even identification of about hundred cosmic TeV gamma-ray sources and measurement of the Ultra-High-Energy Cosmic-Ray flux. At least few tens of the identified TeV gamma sources in the Galaxy are expected to be also high-energy neutrinos sources. Many other extragalactic sources, not seen in TeV gamma-rays, may also be high-energy neutrino emitters. Neutrinos, light and uncharged, are very promising probes for high-energy astrophysics since they can reach the Earth from cosmic distances and from astrophysical environments obscure to high-energy gammas and nuclei. Theoretical estimates indicate that a detection area of the order of a few km^2 is required for the measurement of HE cosmic ν fluxes. The underwater/ice optical Čerenkov technique is widely considered the most promising experimental approach to build high-energy neutrino detectors in the TeV-PeV energy range. After the first generation of underwater/ice neutrino telescopes (Baikal, AMANDA and ANTARES), the quest for the construction of km^2 size detectors have already started. At the South Pole the construction of the IceCube neutrino telescope is in an advanced stage, while the ANTARES, NEMO and NESTOR collaborations together with several other European Institutions take part to KM3NeT aiming at the installation of a km^3-scale neutrino telescope in the Mediterranean Sea. Also limits for UHE neutrino detection were strongly improved in the last few years, especially with the recent results of ANITA and Auger. IceRay, a very large detector based on the radio-acoustic technique at the South Pole, has been proposed. Intense R&D activities are also ongoing on thermo-acoustic techniques that could provide a viable solution for UHE detection underwater. This paper reviews the status and perspectives of high-energy neutrino astronomy from an experimental point of view.

PACS `95.85.Ry` – Neutrino, muon, pion, and other elementary particles; cosmic rays.
PACS `98.70.Sa` – Cosmic rays (including sources, origin, acceleration, and interactions).
PACS `13.85.Tp` – Cosmic-ray interactions.
PACS `29.40.Ka` – Cherenkov detectors.

1. – Introduction

The understanding of the violent side of the Universe is a major challenge in astroparticle physics. Indeed observations of the diffuse photon flux at the Earth indicate that the energy content in X- and γ-rays, produced by violent phenomena, is comparable to that associated low-energy phenomena. However the comprehension of the High-Energy (HE) Universe is very limited.

The messengers of the high-energy Universe are hadrons (protons and heavier nuclei), gamma-rays and neutrinos. Moreover, since some astrophysical objects such as SuperNovae and Gamma-Ray Bursts are connected to the acceleration of huge macroscopic masses, therefore gravitational waves are also expected to play an important role [1]. Each of these probes reveals peculiar behaviours of cosmic sources but only an astronomy based on contemporary observation of astrophysical objects with different techniques will allow to get a deeper insight into the HE Universe and into the mechanisms responsible for the production of high-energy particles. In particular, the most appealing feature of neutrinos —chargeless particles interacting only weakly with matter— with respect to protons and gammas, is that they can travel through the Universe without being deflected or absorbed. Figure 1 shows the absorption length of protons and gamma-rays in the Universe as a function of energy: the Very-High-Energy (VHE, $10^{12}\,\text{eV} < E < 10^{15}\,\text{eV}$) photon horizon is limited to few tens Mpc by the interaction on the diffuse cosmic microwave and

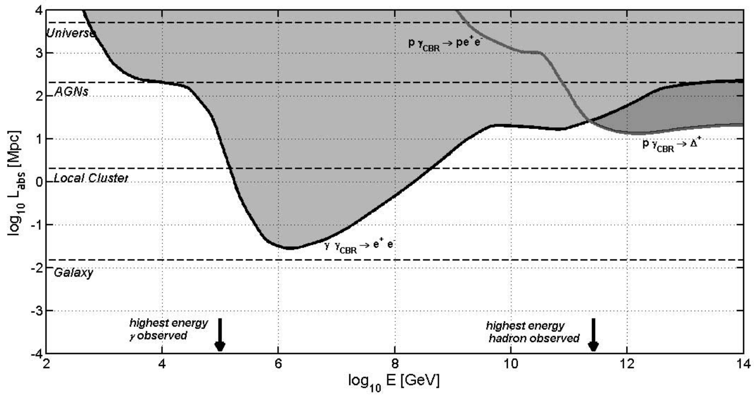

Fig. 1. – Absorption length of protons and gammas in the Universe as a function of particle energy. The gray shaded areas indicate the region not accessible to proton and gamma astronomy.

infrared background; ultra-high-energy protons are absorbed within 100 Mpc by their interaction with the Cosmic Microwave Background Radiation (CMBR), named, after the scientists Greisen, Zatsepin and Kuzmin, GZK effect [2, 3].

Neutrino astronomy will therefore open a new window on the "violent" Universe. In fig. 2 we show the differential spectrum of neutrinos (times E^2) measured or expected at the Earth as a function of neutrino energy. A flux of cosmic neutrinos, called Cosmic neutrino Background originated in the first stages of the Universe analogously to the CMBR [4], has such a low-energy that in spite of the fact that they are extremely abundant in the Universe, it cannot be detected with the present or planned detector. In the MeV-TeV energy regime, the scenario is nowadays clear enough: solar [5-7] and

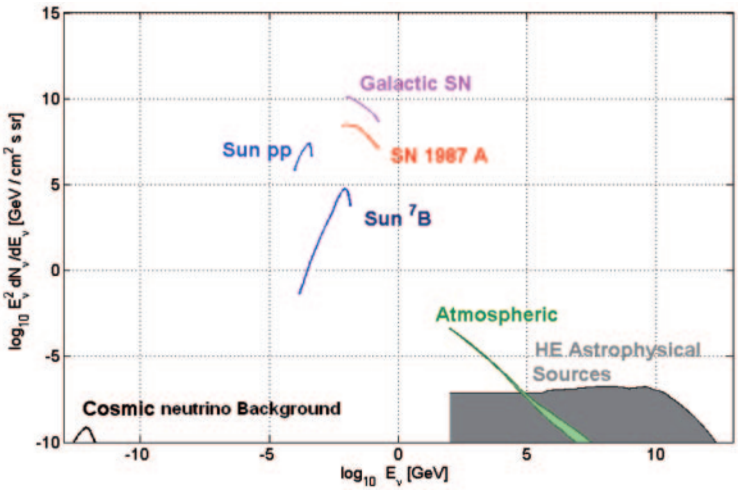

Fig. 2. – Neutrino fluxes at the Earth. Only neutrino fluxes from the Sun, SuperNova 1987A and atmospheric neutrinos have been measured. The low-energy (cosmic neutrinos) and high-energy ranges are still experimentally unexplored.

atmospheric neutrino fluxes [8] are determined with good accuracy, uncertainty remains on SuperNova (SN) neutrinos, for which our knowledge relies only on about 20 $\bar{\nu_e}$ events observed in coincidence with the SN1987A explosion [9-11]. The detection of HE neutrinos ($E_\nu > 1\,\mathrm{TeV}$) should allow to extend our knowledge to the far high-energy Universe and to probe the dense core of the most powerful cosmic accelerators. The price to pay is that neutrinos are extremely difficult to detect and therefore the opening of high neutrino astronomy requires huge detectors.

Theoretical expectations on high-energy neutrino fluxes vary a lot according to different models, a large part of the uncertainties being due to the incomplete knowledge of the astrophysical objects, therefore more robust estimates are obtained extrapolating available experimental data.

In particular, estimates of the diffuse neutrino fluxes and of the so-called BZ (Berezinky-Zatsepin) neutrino flux at Ultra High Energies (UHE, $E > 10^{15}\,\mathrm{eV}$) and Extremely High Energies (EHE, $E > 10^{18}\,\mathrm{eV}$) —produced as a consequence of the GZK effect— can be obtained on the basis of the measured Cosmic Rays (CR) [12]. On the other hand, in the hypothesis of hadronic processes and sources transparent to high-energy gamma-rays, neutrino fluxes from specific point-like sources can be derived from the observed gamma TeV emission. Both kinds of observations indicate that masses of target media of the order of few GTon are needed, and up to hundreds of GTon for EHE neutrinos ($E_\nu > 10^{18}\,\mathrm{eV}$). The use of natural media as ν target is therefore mandatory to build such detectors with affordable budget.

In this review we trace the history, status and perspectives of high-energy neutrino astronomy with emphasis on the experimental point of view. Moreover, we also summarize the main experimental evidence concerning CR and VHE gamma-rays that are relevant for high-energy neutrino detection as well as the current understanding about the most promising of the candidate high-energy neutrino sources.

2. – The cosmic-rays spectrum

Cosmic-rays (CR), whose first studies date back to the beginning of XX century [13,14] are still a puzzling subject for physicists. Up to date measurements show that CR flux extends over 10 orders of magnitude in energy, up to $3 \cdot 10^{20}\,\mathrm{eV}$, and over 28 orders of magnitude in flux, down to few particles per $100\,\mathrm{km}^2$ per century. The measured composition of the bulk of CR is hadron dominated, with about 87% protons, 9% alpha-particles and the rest shared among heavier nuclei, photons and electrons [15].

The low energy region of CR spectrum ($E_{CR} < \mathrm{GeV}$) is well explained by solar activity; above a few GeV the CR energy spectrum follows a power law with spectral index $\alpha \simeq 2.7$ as show in fig. 3 [16]. For clarity sake in fig. 3 we also show the CR spectrum multiplied by $E^{2.7}$, that reveals the presence of different trends with increasing energy. At $E < 10^{14.5}\,\mathrm{eV}$ the CR spectral index is $\alpha \simeq 2.7$, between $E \simeq 10^{14.5}\,\mathrm{eV}$ and $E \simeq 10^{17.5}\,\mathrm{eV}$ the spectral index becomes softer ($\alpha \simeq 3$), above $E = 10^{18.5}$ the spectral index changes again to $\alpha \simeq 2.7$. The two breaks in the energy spectrum are usually referred as *knee* and *ankle*, respectively. Above $E \simeq 10^{19}\,\mathrm{eV}$, the CR flux measured at the Earth is as low as 1 particle/(km^2 year), and above $10^{20}\,\mathrm{eV}$ the CR spectrum is suppressed.

In spite of the fact that CR spectrum has been measured with great accuracy up to $10^{20}\,\mathrm{eV}$, a conclusive evidence of connection with sources is still missing. The arrival direction at the Earth of cosmic rays, mostly composed by protons and nuclei is, in fact, randomized by the Galactic ($B \simeq 3\ \mu\mathrm{G}$) and intergalactic ($B \simeq \mathrm{nG}$) magnetic fields. The gyro-radius of a nucleus having charge Z and Energy E_{18} (that is expressed in units

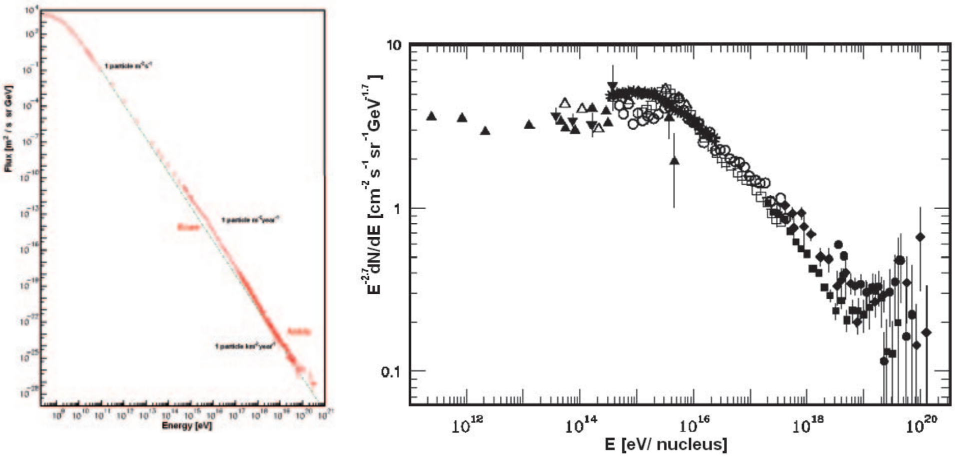

Fig. 3. – Left: The measured cosmic-ray spectrum as a function of energy [15]. Right: The CR spectrum multiplied by $E^{2.7}$; two main changes of the spectral index occur at $E \simeq 10^{14.5}$ eV (*knee*) and at $E \simeq 10^{14.5}$ eV (*ankle*), see text [16].

of 10^{18} eV) is

$$R_{gyro}(E) = E/Z \times B_{Galaxy} \simeq 400 \cdot E_{18}/Z[\text{pc}]. \tag{1}$$

For a $E \simeq 10^{18}$ eV proton, R_{gyro} is comparable with the thickness of the Galactic-disk Halo ($\simeq 200$ pc) and much smaller than the Galactic-disk radius ($\simeq 15$ kpc). This implies that pinpointing of CR sources is possible only with protons having $E_p > 10^{19}$ eV.

The bulk of CR spectrum is understood in terms of particles accelerated in astrophysical sources through the Fermi acceleration mechanism [17]. This mechanism (whose theoretical description was revised in a more effective version by Bell [18]) takes place in sources where a plasma of charged particles (e^+e^- or/and p^+e^-) is contained by strong magnetic fields and is driven by strong shock waves. Charged particles gain energy, statistically, crossing the shock front from the downstream to the upstream region and viceversa, as shown in fig. 4. The expected spectrum of Fermi accelerated particles follows an $E^{-(2-2.2)}$ power law and the maximum energy that a particle can reach is a function of the confinement time within the shock. Since confinement is a function of the object dimensions and strength of the magnetic field, Hillas [19] provided an useful rule of thumb to estimate the maximum energy that a charged particle can reach in a shock:

$$E_{max} \approx \beta_{shock}\, Z\, B_{\mu\text{G}}\, R_{\text{kpc}}[\text{eV}], \tag{2}$$

where Z is the particle charge in units of e, $\beta_{shock} \times c$ is the shock wave velocity, B and R are the source magnetic field and the source linear extension, respectively.

Several astrophysical environments were identified as possible candidates where the Fermi acceleration mechanism can take place. Among all, SuperNova Remnants (SNR), Active Galactic Nuclei (AGN) and Gamma-Ray Burst (GRB) seem to play a major role. Figure 5 groups classes of astrophysical objects as a function of magnetic field B and size R. Only sources for which the product $B \times R$ is above the displayed lines (see eq. (2)) can accelerate protons up to the corresponding energy.

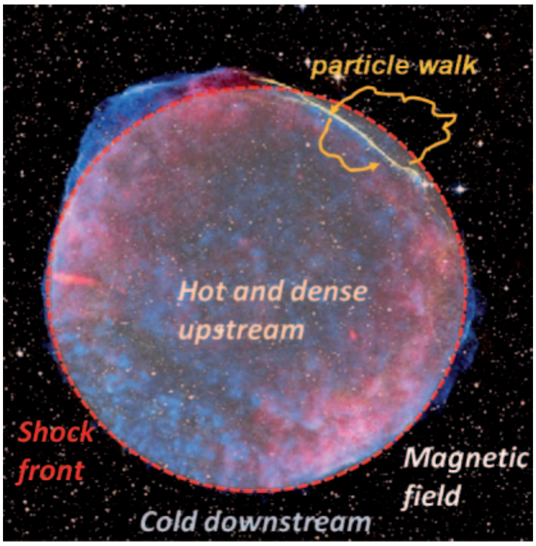

Fig. 4. – The Remnant of SN1006 observed by the Hubble Space Telescope (visible) and by the Chandra satellite (X-rays). Shocks of SuperNova Remnants are indicated as responsible of CR acceleration in the Galaxy.

In the following a discussion about experimental data and candidate CR sources is presented.

A number of arguments indicate that Galactic SNRs are the most probable sources of the CR flux below the ankle. Several observations indicate that the chemical composition of the CR flux, in this energy range, is largely dominated by protons till the knee energy, then, with increasing energy, He, the CNO group, Si, Mg and, at last, Fe dominate. These nuclei are the ones synthesized by nuclear-fusion processes occurring in different stages of massive stars evolution and then spread out in the Galaxy during the SN explosion. Another hint is provided by energetics [20]. The luminosity of Galactic SNs,

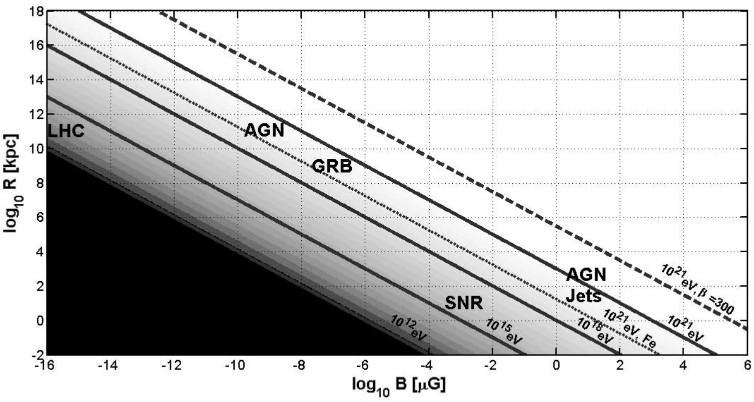

Fig. 5. – The Hillas Plot. Astrophysical sources accelerate high-energy protons and nuclei through diffuse shock acceleration. The particle maximum energy is a function of the source dimensions and magnetic field.

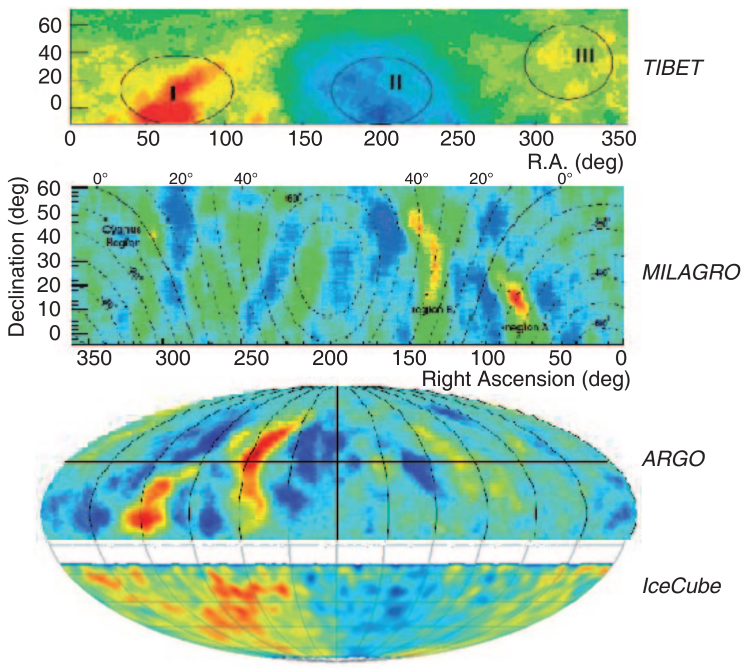

Fig. 6. – Anisotropy in the Cosmic Ray arrival direction is now observed by (from top to bottom) Tibet, MILAGRO, ARGO and IceCube (muons). The color scale refers for the Tibet experiment (2001–2005) to CR flux relative intensity (violet $-3 \cdot 10^{-3}$, red $+2 \cdot 10^{-3}$), for the other experiments color refers to statistical significance in units of standard deviations: Tibet MILAGRO (7 years, blue: 5σ, red: 15σ), ARGO (424 days; blue: 7.6σ, red: 11.4σ), Icecube (22 strings, 1 year; blue: -5σ, red: $+5\sigma$).

assuming an average energy release of 10^{51} erg per SN and an explosion rate of 1/30 years, is $L_{SN} \simeq 10^{42}$ erg/s. On the other hand, the integral power of observed CR, in the energy range between 1 GeV and 10^{16} eV, is $P_{CR} \simeq 10^{40}$ erg/s. This value is consistent with a fraction of few percent of L_{SN}, in good agreement with the estimated conversion efficiency of the Bell-Fermi model for SNR shocks. In this scenario protons are accelerated to very high energies in SNR and their energy spectrum follows the Bell-Fermi $\simeq E^{-(2-2.1)}$ distribution, times a factor $\tau(E) \propto E^{-0.6}$ due to confinement time in the Galaxy, in agreement with the observed $\alpha \simeq 2.7$ spectral index [21].

Nevertheless the question whether only SNRs shocks are responsible for a "local" acceleration of CR, or the statistical acceleration process takes place in a distributed way in the whole Galaxy or in active region such as superbubbles is still open [22].

As expected (eq. (1)), in this energy region, the sky-map of CR is isotropic due to randomization of charged particle arrival direction in the Galactic magnetic field. However, recently, the MILAGRO experiment observed two with a fractional excess of about 6×10^{-4} and 4×10^{-4}, respectively, from the directions corresponding to $\delta = -20°$, $70° < RA < 80°$ (named region A) and $30° < \delta < 40°$, $130° < RA < 150°$ (named region B) [23]. The Tibet [24] and ARGO [25] experiments also observed these anisotropy and more recently even the IceCube neutrino telescope [26] showed anisotropy of cosmic-muon arrival direction in the corresponding Southern Hemisphere regions (see fig. 6), however a clear explanation of these observations is still missing. MILAGRO also observed a "hot spot" of $E > 10\,\text{TeV}$ gamma rays, in the direction of the Cygnus region, that could be explained by the presence of active cosmic ray sources accelerating hadrons which interact with the local dense interstellar medium and produce gamma-rays through pion decay [27].

Above the knee energy the total CR flux decreases and the composition increases in metallicity as expected in the scenario of SNR acceleration: protons are not confined any more in the Galaxy, and only nuclei with higher Z remains trapped in the Galaxy.

At $E > 10^{18.5}\,\text{eV}$ (the *ankle* region) the CR spectrum features change again. Above this energy the CR flux similar to the pre-knee region: the spectral index is close to 2.7 and the flux measured by AGASA [28] and HIRES [29, 30] experiments appears to be proton-dominated, though experimental data from the Pierre Auger Observatory (PAO, hereafter Auger) detector seem to favor a mixed composition [31]. Since the known Galactic sources (SNR, Microquasars, Pulsar Wind Nebulae) cannot accelerate particles to extremely high energies, as shown in eq. (2), the detection of cosmic protons with energies up to $E > 10^{19}\,\text{eV}$ suggests the presence of extragalactic accelerators. According to eq. (2) there are only few classes of cosmic objects capable to accelerate protons at $E >$ EeV ($10^{18}\,\text{eV}$), among these Gamma-Ray Bursters (GRB) [32] and powerful Active Galactic Nuclei (AGN) [33] are the most favorable candidates. These sources are, respectively, the most luminous bursting ($L_{GRB} \simeq 10^{53}\,\text{erg/s}$) and the most luminous steady ($L_{AGN} \simeq 10^{46}\,\text{erg/s}$) objects in the Universe ever observed. Protons having $E \geq 10^{19.5}\,\text{eV}$, likely accelerated in AGNs and GRBs, are considered good astrophysical probes being only slightly bent by cosmic magnetic fields. Experimental results concerning a possible correlation between UHE proton arrival directions and AGNs are, however, controversial.

Results published by the Auger collaboration in 2007 [34] indicated a correlation between the Veron Cetty Veron (VCV) AGN catalog [35] and the arrival direction distribution of events with $E \geq 56\,\text{EeV}$, with $\phi = 3.1°$ and redshift $z_{max}^{AGN} = 0.018$(1), while the probability of random correlation is as small as 10^{-5}. However, the correlation claimed by the Auger Collaboration is in contrast with the isotropic distribution measured by HIRES with no evidence of clustering. The most recent analysis of the correlation between the arrival directions of the highest cosmic rays ($E \geq 55\,\text{EeV}$) for the whole present set of Auger data [36] indicates, for the 58 observed events, a weaker degree of correlation with nearby quasars and active galactic nuclei of the VCV catalogue than previously observed, while the overlap with the SWIFT-BAT AGN catalogue [37] is stronger, as shown in fig. 7.

Others authors [38] suggest, in the hypothesis of a stronger intergalactic magnetic field, a correlation, within 10 degrees, of 9 over the 27 observed events ($E > 56\,\text{EeV}$) with the close ($\simeq 5\,\text{Mpc}$) source Centaurus A (see subsect. **5**·1), an interesting region with many potential sources. The excess of events in the direction of the radio source Cen A, from updated Auger data is shown in fig. 7 [36].

Above $10^{20}\,\text{eV}$ the CR flux is expected to be suppressed by the GZK effect [2,3]. Since AGNs and GRBs lies at cosmological distances, protons and nuclei accelerated in these sources are absorbed during their journey to the Earth by interaction with the Cosmic Microwave Background Radiation (see fig. 1).

(1) The distance of an object at redshift z corresponds to $4.2 \cdot z$ Gpc, assuming the Hubble constant $H_0 = 71\,\text{km}\,\text{s}^{-1}\,\text{Mpc}^{-1}$.

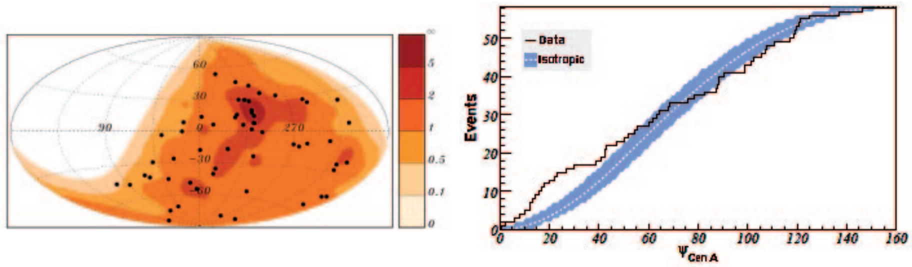

Fig. 7. – Left: The sky map, in Galactic Coordinates, of Auger events up to March 2009. The black dots represent the 58 events with $E > 5.5 \cdot 10^{19}$ eV. Brownish areas represent the distribution of AGN observed by the SWIFT-BAT satellite [37]. Right: Cumulative number of Auger events with $E > 56$ EeV as a funtion of distance from Cen A. The average isotropic expectation is also shown (white dotted line) together with 68% confidence level interval (blue area).

Since the cross-section of the proton photo-pion production $p + \gamma \to N + \pi$ is $\sigma_{p\gamma}$ is $\simeq 100$ μbarn and the average CMBR density is $n_{CMBR} \simeq 400$ *photons* cm^{-3}, the absorption length of EHE protons in the Universe is roughly

$$L_{p,CMBR} \simeq (\sigma_{p\gamma} \cdot n_{CMBR})^{-1} < 50\,\text{Mpc}, \tag{3}$$

well shorter than the distance between cosmological sources and the Earth.

The observation of a suppression in the ultra-high-energy region of the CR energy spectrum is confirmed both by HIRES [39] and Auger [40], while in AGASA data [28], now under revision, the suppression was not observed. However, the most recent analysis of the Auger data, including all the events collected up to March 2009, the interpretation of the Ultra —or Extremely— High Energy Cosmic Ray (UHECR, EHECR) spectrum in terms of GZK effect cannot be firmly established.

Indeed several independent analysis, concerning the mass composition of Auger events $E > 3$ EeV (collected up to March 2009), show a trend as a function of the maximum number of electromagnetic particles of a shower with energy E and mass A reached at a depth X_{max} 8 that suggests an increase of the mean primary mass with increasing energy [41, 42]. Moreover, the trend of the X_{max} root mean square values, RMS-X_{max} reported for the Auger data, indicates that the most energetic CR are heavy nuclei. The Auger UHECR mass composition shows a completely different trend respect to the HIRES [30] detector data that look compatible with a proton dominance in the mass composition of UHECR (see fig. 8). The recent Auger results raise several different questions going from the maximum energy achievable in cosmic accelerators to our knowledge of the proton cross at these extreme energies. However, the strong disagreement between the observations of the two biggest experiments in UHECR represents a major (disappointing) puzzle in UHECR [43]. In conclusion, the knowledge of the mass composition of UHECR, is an extremely relevant piece of information not also for the understanding of the mechanisms involved in the production of the most energetic cosmic rays, but also for the possibility of doing proton astronomy to investigate the violent Universe.

In conclusion, even in the hypothesis of composition dominated by protons, the proton bending due to cosmic magnetic fields and the GZK effect, shrinks the energy and distance region accessible to UHE proton astronomy between $\simeq 10^{19.5}$ eV and $\simeq 10^{20.5}$ eV and few hundreds Mpc in distance.

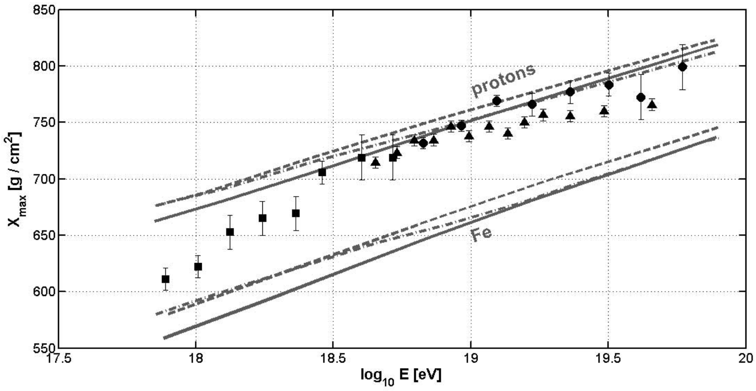

Fig. 8. – Mass composition of UHECR as a function of reconstructed energy. Data from Auger (triangles), HIRES-MIA (squares) and HIRES 2009 (circles) compared with different QGSJET simulations. QGSJET01 (solid), QGSJET02 (dotted), QGSJETII (dash-dotted) for protons and iron nuclei. See also ref. [43].

On the other hand, the mass composition and the observation of the GZK are also a crucial issue for neutrino experiments aiming at the detection of the so-called GZK (or BZ) neutrinos: the presence of the GZK cut-off would lead to the production of a cosmological flux of "guaranteed" ultra-high-energy neutrinos, that can be observed at the Earth with features depending on the CR flux and composition, as discussed in the following.

3. – Cosmic gammas and neutrinos at $E \geq$ TeV

After the observations of the first generation IACT (Imaging Air Čerenkov Telescopes) CANGAROO [44], Whipple [45] and HEGRA [46], that detected a few intense VHE sources such as the Crab Nebula and the close AGN Mkn-501, in recent years the TeV gamma-ray sky has become "bright". The advent of the second-generation IACT such as MAGIC [47], the stereoscopic systems HESS [48] and VERITAS [49], and the operation of MILAGRO and ARGO experiments, allowed a detailed survey of the TeV gamma-ray sky and lead to the discovery of about 100 TeV gamma sources [50, 51].

Very-High-Energy gamma-ray emission from astrophysical sources is historically interpreted through electromagnetic mechanisms, namely the inverse Compton scattering of Fermi-accelerated electrons/positrons on the low-energy radiation field produced by synchrotron emission of charged particles. The latter seem to be the case of Galactic Pulsar Wind Nebulae (PWN) or of the close AGNs Mkn-421 and Mkn-501 [52], whose emissions have been studied for several years.

However, hadronic processes seem now to play a major role in several of the observed TeV gamma-ray sources. In this scenario, protons accelerated via Fermi mechanism, interact with ambient radiation and/or matter, within the source or with nearby gas clouds producing pions. Neutral pions then decay into a pair of γs, while charged pions decay producing neutrinos. In the case of interaction with ambient radiation, the reaction

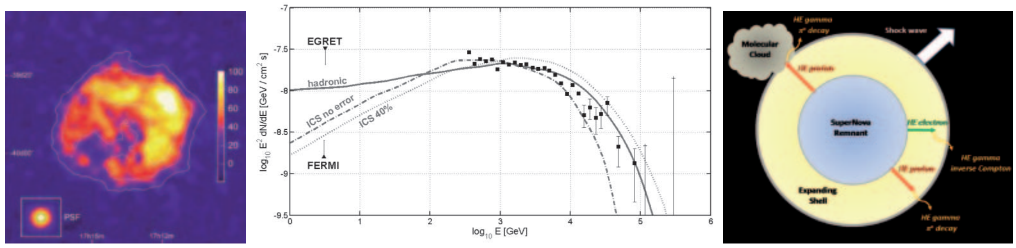

Fig. 9. – Left: Contour map of gamma-rays counts from SNR RXJ1713.7-394 detected by HESS (threshold $E_\gamma = 800\,\text{GeV}$), the solid lines indicates the X-ray surface brightness as seen by ASCA and ROSAT in the 1–3 keV range. Centre: Average spectral index of photons as a function of energy. Right: The HESS observation suggests a scenario in which CRs are accelerated in SNR and subsequently interact in the superposition region between SNR shells and a close-by Molecular Cloud [48].

chain is the following:

$$
\begin{array}{llll}
 & & \pi_0 \rightarrow \gamma + \gamma & \\
 & \Rsh & & \\
p + \gamma \rightarrow N+ & \pi & & \\
 & \Lsh & & \\
 & & \pi^\pm \rightarrow \nu_\mu + \mu & \\
 & & & \Lsh \\
 & & & \mu \rightarrow e + \nu_\mu + \nu_e .
\end{array}
\tag{4}
$$

Roughly speaking the threshold of the $p\gamma \rightarrow N\pi$ reaction is $E_p \simeq 300\,\text{MeV}$ in the center-of-mass reference frame, assuming the main contribution due to the Δ^+ resonant channel, and the pion carries about 20% of the proton energy.

The expected "hadronic" gamma flux (produced in the $\pi^0 \rightarrow \gamma\gamma$ channel) therefore follows a E^{-2} power law, as the primary Fermi proton flux, within the energy region constrained, at low energy by the Δ^+-resonance threshold and, at high energy, by E^p_{max} achievable in the cosmic accelerator. Similarly a muon neutrino flux is produced, with a spectrum E_ν^{-2} and average energy $E_\nu \simeq 5\% E_p$. If the muon cooling time in the source is larger than the muon decay time, high-energy electron neutrinos are also produced with a production ratio of 2:1 (see eq. (4)). Taking into account neutrino flavor oscillations during the source-Earth journey, equipartition between the three leptonic flavors $N_{\nu_\mu} : N_{\nu_e} : N_{\nu_\tau} = 1:1:1$ is expected at the Earth.

The observation by the HESS telescope of TeV gamma rays emitted by the ROSAT and ASCA X-Ray source RXJ1713.7-3946 [48], indicated, for the first time, features suggesting the presence of proton Fermi acceleration. In fig. 9 the gamma-spectrum of the source, measured by HESS is reported. The measured spectral index $\alpha \simeq 2.1$ and the morphology of the source favorably indicate a scenario of Fermi-accelerated protons interacting on a dense molecular cloud in the NW region close to the source.

For this source another interesting piece of information could be provided by the FERMI satellite [53] data that will observe gamma-rays in the energy region between 1 and a few tens of GeV. As shown in fig. 9, the forthcoming observations will probe a region where hadronic and leptonic emission are expected to produce different gamma spectra putting perspectives to discriminate between these two mechanisms on a firm ground and consolidating the neutrino flux expectations.

Another class of promising hadronic sources is formed by the TeV gamma sources that have no counterpart in other wavelengths, for this reason, called "Dark Accelerators". The number of these sources is, to date, about 20 [54]. However, also for these sources, purely electromagnetic processes cannot be definitively ruled out [55] and only the detection of high-energy neutrinos will provide the ultimate "smoking gun" to demonstrate the occurrence of hadron acceleration processes.

Moreover the horizon of $E_\gamma \geq 10\,\text{TeV}$ gamma-rays is about 100 Mpc, this limits VHE gamma telescopes to the observation of the Galaxy and of the close Universe (see fig. 1). The observation of astrophysical neutrinos will, therefore, open a window on the far high-energy Universe, where AGN and GRB emissions are expected to play a major role.

As discussed above, the scenario in which astrophysical sources are the accelerators of the observed hadronic cosmic rays, is nowadays strongly supported by several TeV gamma-ray observations. In the following we will describe the astrophysical environments proposed as sites for cosmic-ray acceleration, VHE gamma-rays and neutrino production. The sources presented in the following are candidates for HE neutrino production and, some of them, are expected to produce ν fluxes high enough to be detected by a km^3-scale detector. For clarity's sake we will deal with Galactic and Extragalactic sources separately.

The first one are less luminous and less powerful, but thanks to their proximity to Earth, they could generate neutrino fluxes that can be observed as point-like sources. Moreover, in the hypothesis of hadronic emissions, the detected TeV gamma fluxes, provide a rather reliable estimate of the high-energy neutrino fluxes.

Extragalactic sources are expected to produce neutrino fluxes extending up to Ultra High Energies, that will emerge above the atmospheric diffuse flux. The most luminous ones are also candidate for point-like observation.

4. – Candidate Galactic high-energy neutrino sources

The operation of HESS [56], MAGIC [57] and the other γ TeV telescopes disclosed the very-high-energy gamma-ray sky, revealing a large number of TeV sources. Due both to gamma-ray absorption in the Universe and closeness to the Earth, a large part of these sources are harbored in the Milky Way [58] (see fig. 10).

Galactic TeV gamma-ray sources are mainly associated with SNR and X-Ray Binaries and with their jetty subclasses: Pulsar Wind Nebulae (PWN), that were found to be the dominant species γ TeV emitters in our Galaxy, and microquasars [50]. In particular SNR and microquasars show peculiar TeV gamma emission that suggests interaction of accelerated protons on dense media or local radiation field, that could also produce TeV neutrino fluxes [59].

4˙1. *Galactic Supernova Remnants.* – The gas of SNRs is a large reservoir of kinetic energy where diffusive shock waves is supposed to accelerate protons and electrons.

Electron acceleration up to tens of TeV is demonstrated by the observation of X-rays and gamma-rays from SNR associated to Pulsar Wind Nebulae [60]. The CRAB Nebula, Kookaburra, G21.5-0.9, MSH15-5 2 and HESS J1825-137 [61] are only few, known examples. In these sources the rotational energy of the spinning-down neutron star (pulsar), that emerges from the SN explosion, is converted into a pulsar wind: a relativistic plasma of electrons and positrons. The pulsar wind terminates in a shock when it encounters

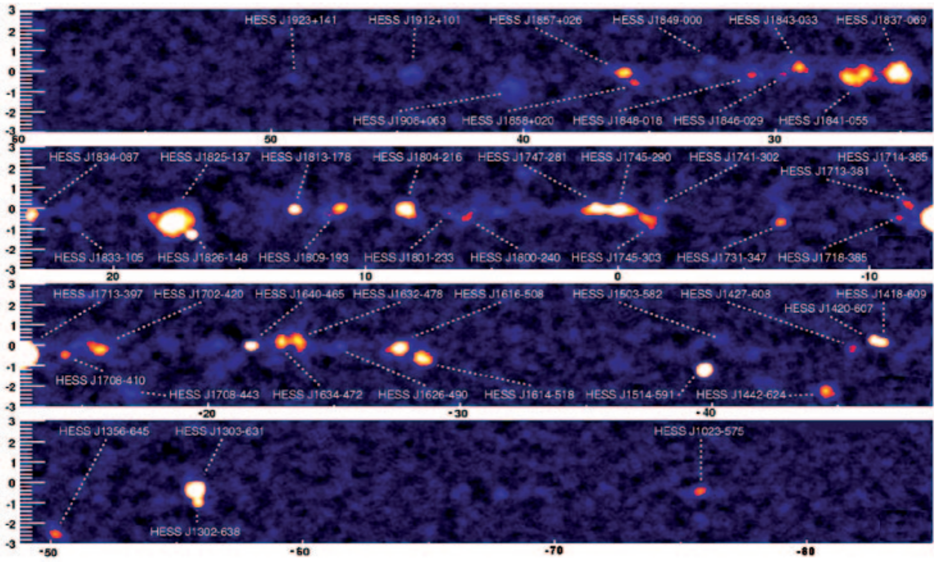

Fig. 10. – Distribution of TeV gamma-rays in the Galactic-plane region observed by HESS, Galactic-plane survey 2008 [58].

the ambient medium, *e.g.* the SN ejecta. Within this magnetised environment, e^+ and e^- emit both synchrotron X-rays and TeV energy gamma-rays, by up-scattering (inverse Compton scattering) on ambient photons, *e.g.* microwave background [62].

On the other hand, a direct evidence of efficient proton acceleration is still missing. A breakthrough discovery was the detection of narrow and bright X-ray filaments in some SNR shells, associated to very high energy electrons entering an intense magnetic field environment (up to few mG) [63]. Such large magnetic fields are suggested to be the result of charged particle streaming from upstream to downstream in shocked SNR ejecta (or in the interstellar medium, during the Sedov phase of the shock). In this conditions electrons are quickly cooled down due to synchrotron emission — thus the VHE gamma flux from inverse Compton is strongly suppressed — while protons are efficiently accelerated to energies $> 1\,\mathrm{PeV}$. The expected proton flux follows a power law spectrum with $\alpha = 2.0$–2.2 and a cutoff energy $E_c \simeq 10^{14}$–$10^{18}\,\mathrm{eV}$, which depends on the age of the SNR [64]. Another interesting piece of information was recently provided by Helder *et al.* [65], who determined that, in SNR RCW86, a high cosmic-ray pressure must be considered to explain the X-ray emission from the NE part rims of the source.

The interaction of Fermi protons with matter target of the SNR shells leads to the production of pions and therefore to VHE gamma and neutrinos as previously discussed.

The detection of gamma rays up to $E_\gamma \simeq 100\,\mathrm{TeV}$ from SNR RXJ1713.7-3946 [48] and other similar sources, such as Vela Jr (RXJ0852.0-4622) [66], showing power law gamma-ray spectra with $\alpha \simeq 2$–2.2 provides therefore a strong indication of SNRs as CR sources.

Going deeper in details, present data suggest that the SNR gas environment is typically transparent to CR, being the matter density n of SNR shells too small for efficient proton-proton interaction ($n \simeq 1$ particle/cm^3). The production of pion-induced gamma-rays is therefore inefficient. On the other hand, the presence of massive Molecular

Clouds ($M_{MC} > 10^2 M_\odot$) close to the SNR provides a much denser target for interaction of the Fermi-accelerated protons, being the matter density in these environments $\simeq 100$ particles/cm^3. Molecular Clouds can be kept by the SNR wind during its expansion, as in the case of RX J1713.7-3946, or "illuminated" by the CR stream accelerated within a nearby SNR [67]. This latter, seem to be the case of the so called "Dark Accelerators" or "Unidentified Sources" detected by TeV gamma-ray telescopes without, or with very faint, counterpart in other photon wavelengths.

Several observations of TeV gamma-rays sources are now associated to galactic SNR expanding close to Molecular Clouds, identified looking at their H2, CO or OH maser emissions. Typical cases are SNR W28, W51C [54, 68], CTB37A and CTB37B [69]. It is not yet possible, however, to exclude that, at least part of, the observed TeV gamma radiation is produced by electromagnetic processes. The ultimate proof that SNRs effectively accelerate CR will be obtained by the observation of high-energy neutrinos.

Using a phenomenological approach Vissani, Villante and Costantini [70, 71] determined the CR flux accelerated by SNR, required to produce the observed TeV gamma-ray flux in the hadronic scenario. In this approach the interactions of cosmic-ray protons with a hydrogen ambient cloud result in the production of mesons which subsequently decay producing gamma-rays (from the decay of π_0 and η) and neutrinos (from the decay of charged π and K). Since, both gamma-ray and neutrino fluxes depend linearly on the flux of the primary cosmic-rays, there is a linear relation between photon and neutrino fluxes and one only need to know the relative number of pions, kaons and η's produced by cosmic-ray interactions on the target cloud at any given energy. Taking also into account the effect of neutrino oscillations from the production site to the Earth the authors calculated an upper bound for the muon neutrino and anti-neutrino flux reaching the Earth from the SNR RXJ1713.7-3946, shown in fig. 11.

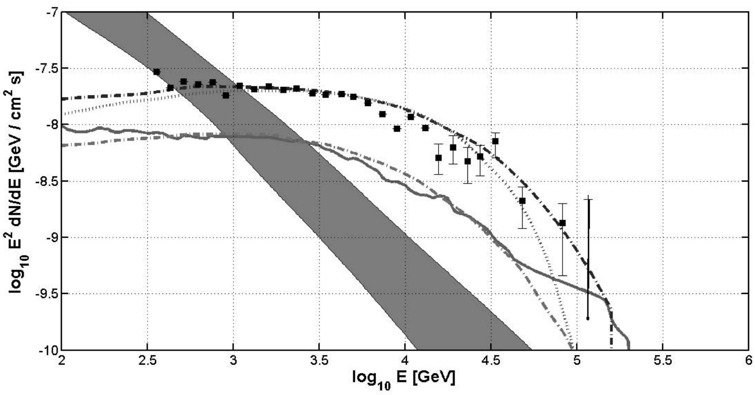

Fig. 11. – TeV neutrino ($\nu_\mu + \bar{\nu_\mu}$) fluxes expected from RXJ1713.7-3946 calculated by Vissani *et al.* (solid line) [71] and Amato *et al.* [72] (light gray dash-dotted line). The HESS data, from combined 2003, 2004 and 2005 source observations (black squares), are shown for comparison together with the hadronic-origin TeV gamma-ray flux calculated by Amato *et al.* (dark gray dash-dotted line) [72] and Berezkho *et al.* (dotted line) [73, 74] is also shown. The solid lines delimiting the shaded area represent the expected atmospheric neutrino background for a 0.5° bin and 1° neutrino search bin respectively.

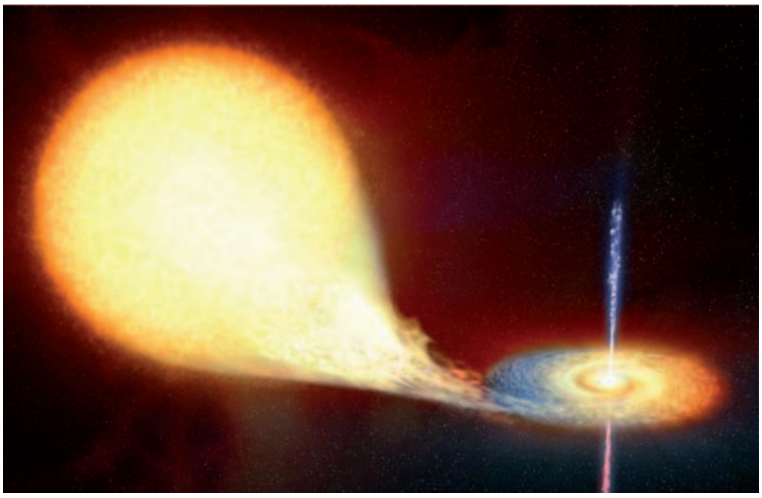

Fig. 12. – Pictorial view of a microquasar: matter flows from the "donor" star to the compact "accretor", which shows relativistic jets.

Amato, Blasi and Morlino [72] have also calculated the expected neutrino (and anti-neutrino) flux from RXJ1713.7-3946, using a non-linear theory of diffusive shock acceleration model to reproduce acceleration of cosmic-rays at Supernova blast wave. Results from their work both reproduce the TeV gamma-ray spectrum measured by HESS and agree with the prediction of Vissani *et al.* (see fig. 11).

4·2. *Galactic X-Ray Binaries and Microquasars*. – X-ray binaries (XRB) are binary stars that produce X-ray emissions. They are typically formed by a compact object called "accretor" (a white dwarf, neutron star, or black hole) and a "donor" star, orbiting around. Microquasars are a subclass of X-ray binaries, formed by a neutron star or a black hole and a star companion in which the compact object exhibits relativistic radio jets [75, 76] (see fig. 12). Mass transfer from the companion star to the compact object, leads to the formation of an accretion disc, and the presence of the jets make them similar to small quasars, hence their name microquasars. Some, like SS433, are persistent sources, while others appear to be intermittent (GRS1915+105 [77]) or periodic (LSI+61.303 [78]).

The observed radiation from microquasar jets, typically in the radio and in some cases also in the IR band, is consistent with non-thermal synchrotron radiation emitted by a population of relativistic, shock-accelerated, electrons. On the other hand, the dominant energy carrier in the jet is unknown, with the exception of the jet of SS433 [79], where the observation of iron X-ray lines and Doppler-shifted H lines indicates a hadronic jet content.

The detection of very-high-energy γ-rays from the LS5039 by HESS [80] ($\Phi_\gamma(E) \simeq 1.2 \cdot 10^{-12} E_\gamma^{-2.1}\,\mathrm{cm^{-2}\,s^{-1}\,TeV^{-1}}$) and from LSI+61.303 ($\Phi_\gamma(E) \simeq 2.7 \pm 0.4 \pm 0.8 \cdot 10^{-12} E_\gamma^{-2.6\pm0.2\pm0.2}\,\mathrm{cm^{-2}\,s^{-1}\,TeV^{-1}}$ between $\simeq 200\,\mathrm{GeV}$ and $\simeq 4\,\mathrm{TeV}$) by MAGIC [81], clearly demonstrates that microquasars are sites of effective acceleration of charged particles to multi-TeV energies. In particular gamma-ray emission from both sources, show the same periodicity (about 4 and about 26 days, respectively) as the measured radio and X-ray high-state emissions [82, 83]. This would favor the hypothesis

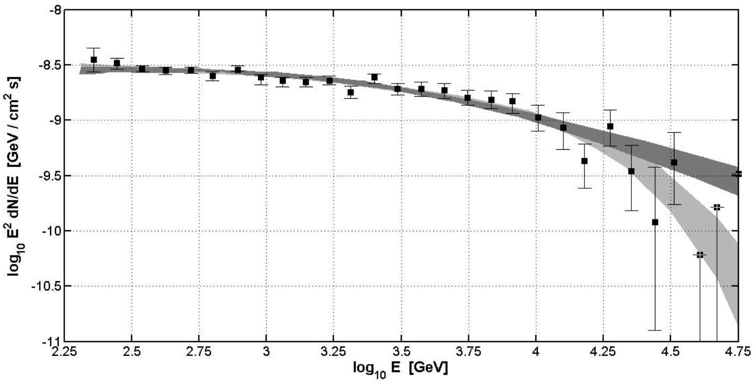

Fig. 13. – TeV gamma fluxes from the Galactic Centre (HESS J1745.290). Both a broken power law (dark gray area) and a power law with exponential cutoff (light gray area) fit the HESS observations.

of gamma-ray production within the binary system, close to the compact object. In this region the intensity of the magnetic field ($B \gg 1$G) strongly limits electron acceleration up to multi-TeV energies, thus favouring a hadronic acceleration scenario [84]. In this case, however, the efficiency of VHE γ-ray production would peak around periastron (the point of closest approach between the two stars), reflecting the minimal separation between particle acceleration sites and targets, and higher target photon densities. This is in contrast with HESS results that show high gamma emission state at the apastron (the point of maximum orbital distance), puzzling the debate on the gamma-ray origin between authors in favor of a leptonic origin for the observed TeV gamma-rays, through electron synchrotron emission followed by inverse Compton scattering, and hadronic model supporters. However, since γ-rays are subject to energy-dependent absorption in the dense low energy photon field of the source [85], both the energy spectrum and the absolute flux of neutrinos, could exhibit a differen behaviour with respect to the detected γ-ray emission.

Levinson and Waxman [86] first proposed the possibility that protons, accelerated at energies > 100 TeV by internal shocks within microquasars jets, could produce TeV neutrinos fluxes through photomeson interaction on ambient X-ray radiation, in a scenario where gamma rays are re-absorbed by pair production with the ambient photon field. Depending on source parameters, Distefano *et al.* [87], calculated that the expected neutrino fluxes range in the interval $\Phi_\gamma(E) \simeq 10^{-12}$–$10^{-10}\,\mathrm{TeV}^{-1}\,\mathrm{cm}^{-2}\,\mathrm{s}^{-1}$. More recently Romero, Christiansen and Orellana [88] proposed a model for LSI+61.303 in which Fermi-accelerated protons in the jet interact with cold protons of the donor stellar wind producing both TeV gamma rays and neutrinos. Aharonian *et al.* [89] estimated, in a hadronic scenario, a minimum neutrino flux of $E_\nu \Phi_\nu(E) \simeq 10^{-12}\,\mathrm{cm}^{-2}\,\mathrm{s}^{-1}$ from LS5039 for $E_\nu > 1$ TeV and much higher fluxes expected in the case of strong γ-ray absorption within the source.

4$\cdot$3. *The Galactic Centre.* – The Galactic Center is a complex environment extending over about 500 pc composed by the candidate super-massive black hole Sagittarius A* (Sgr A*), a population of SNRs and other compact and extended sources and molecular clouds, detected in multiwavelength surveys. The Galactic Centre (GC) region has finally been identified also as an intense source of TeV *gamma*-rays by HESS [90], Whipple [91], CANGAROO [92] and MAGIC [93]. In particular, the recent results of HESS observations of the Galactic Centre region, shown in fig. 13, are compatible with both a power law spectrum with an exponential cut-off and a with broken power law spectrum [94]. The power law spectrum with an exponential cut-off is characterized by a photon index $\alpha = 2.10 \pm 0.04_{stat} \pm 0.10_{syst}$ and a cut-off energy at $E_c = 15.7 \pm 3.4_{stat} \pm 2.5_{syst}$ TeV. The broken power law spectrum exhibits spectral indices of $\alpha_1 = 2.02 \pm 0.08_{stat} \pm 0.10_{syst}$ and $\alpha_2 = 2.63 \pm 0.14_{stat} \pm 0.10_{syst}$ with a break energy at $E_c = 2.57 \pm 0.19_{stat} \pm 0.44_{syst}$. Investigation of possible Quasi Periodic Oscillation activity at periods claimed to be detected in X-rays does not show any periodicity in the HESS signal [95].

Different mechanisms have been suggested to explain the broadband spectrum of the Galactic Centre [96]. Possible associations of the gamma-ray source with the Sgr A East supernova remnant [97] and with the newly detected PWN G359.95-0.04 [98] have been widely discussed in the literature. However, with the reduced systematic pointing error obtained using HESS data up to 2006 [95], Sgr A East is now ruled out to be associated with the VHE emission of HESS J1745.290. The interpretation of the GC TeV signal as annihilation products of dark matter (DM) particles has been discussed in Aharonian *et al.* [99]. The authors find that not more than 10% of the measured gamma flux at $E >$ TeV can be attributed to DM annihilations.

Another possibility is that the supermassive black hole Sgr A* located at the center of the Milky Way is responsible for the VHE emission of the detected HESS J1745.290 source. Stochastic acceleration of electrons and protons may take place in the turbulent magnetic field in the vicinity of Sgr A* [100,101]. These models are able to reproduce the radio, IR and X-ray flaring [102,103]. In addition, they assume that charged particles are accreted onto the black hole, and predicts that a significant fraction of the protons do escape the neighborhood of Sgr A* without undergoing a *pp* collision. Protons presumably diffuse to much larger distances where they can interact with other molecular material producing π_0-mesons, possibly accounting for the observed Galactic ridge emission. This would result in a neutrino flux of the same order of magnitude of the observed gamma flux.

5. – Candidate Extragalactic high-energy neutrino sources

One of the most interesting features of the CR energy spectrum (fig. 3), is the observation of UHECR above the ankle, that calls for the presence of very powerful extragalactic cosmic accelerators. In this section we will summarize the most relevant astrophysical observations concerning Extragalactic sources with special emphasis on Active Galactic Nuclei and Gamma-Ray Burst. We will also present the current status of expectations for the related high-energy neutrino fluxes and expectations for the GZK neutrino fluxes.

Unlike Galactic γ-ray sources, for which the VHE gamma detection —in the hypothesis of hadronic emission mechanisms— provides a rather good estimate of both the expected neutrino flux and its spectral index, the situation is more complex in the case of extragalactic sources. Indeed, the interaction with the Extragalactic Background Light (EBL), that consists of the sum of the starlight emitted by by galaxies through the whole history of the Universe [104], makes VHE γ spectra measured at the Earth much steeper than γ spectra at the source. Moreover, although evidences about the amount of EBL are not conclusive [105] the absorption effect does not allow the exploration of the non-thermal Universe via VHE gamma-rays at distances larger than about 100 Mpc, as already shown in fig. 1.

Neutrino flux estimates from extragalactic sources are therefore very uncertain and rely mostly on theoretical models (for a recent review see [106]).

Starting from the hypothesis that AGNs and GRBs are the dominant sources of CR observed in the energy range 10^{19} eV–10^{21} eV, and that the observed particles are protons, Waxman and Bahcall [107] set a upper bound (the so-called Waxman & Bachall limit) for the high-energy neutrino diffuse flux, that can be detected at the Earth. Their limit, obtained assuming that the energy density injection rate of CR, in the mentioned energy region, is $\simeq 10^{44.5}$ erg $\mathrm{Mpc}^{-3}\mathrm{year}^{-1}$ and that the AGN and GRB proton spectrum at the source follows a E^{-2} power law, is

$$E_\nu^2 \Phi_\nu \simeq \frac{c}{4\pi}\frac{f_\pi}{4}E_p^2\left(\frac{\mathrm{d}N_p}{\mathrm{d}E_p dt}\right)t_{Hubble} \simeq 10^{-7.5}[\mathrm{GeV\ cm^{-2}\ s^{-1}\ sr^{-1}}]. \tag{5}$$

Equation (5) set a "reference" value for the expected neutrino fluxes and set the dimensions of high-energy neutrino telescopes to a km^3-scale, as we will discuss in next sections. However this limit is, as mentioned, strongly related to the composition of the measured CR above 10^{19}, that, as discussed in sect. **2**, appears very uncertain on the basis of the Auger data analysis of the data set 2004-2009.

Astrophysical objects that do not contribute to CR spectrum at Ultra High Energies are not constrained by the WB limit. Among these, galactic sources such as SuperNova Remnants and microquasars and "optically thick" sources (for which the optical depth is $\tau_{p\gamma} \equiv R_{source} \cdot (\sigma_{p\gamma} n_\gamma) \gg 1$) nucleons interact while neutrinos can escape giving rise to a neutrino flux not constrained by eq. (5). This limit does not apply also to a different kind of processes, known as *top-down*, which foresee the production of high energy CR, gammas and neutrinos by the decay or annihilation of particles with mass $M_X > 10^{21}$ eV, relics of the primordial Universe such as: Topological Defects or GUT-scale mass WIMPS (Weakly Interactive Massive Particles)([2]).

A more detailed discussion on the most promising Extragalactic neutrino candidate sources is presented in the following.

5˙1. *Active Galactic Nuclei.* – Active Galactic Nuclei (AGN), the most luminous persistent objects observed in the sky, are galaxies whose electromagnetic radiation has luminosity of the order of 10^{46} erg/s.

The standard scenario for AGNs assumes the presence of a very massive central black hole (10^6–$10^8 M_\odot$) swallowing huge quantities of surrounding matter from an accretion disk and two relativistic jets where particles are accelerated up to the highest energy.

The commonly used classification scheme for AGNs is based on the anisotropy of their emission with respect to the observer: depending on the observation angle AGNs are classified as quasars, Seyfert galaxies, BL Lacs, and blazars, as shown in fig. 14, [109]. Different features of the detected photon spectrum lead to more detailed classification. Although most of AGNs are radio-quiet, a particular ensemble of AGNs are Radio galaxies where the radio emission, due to the synchrotron process, far exceed the luminosity at other wavelengths. Both radio-loud and radio-quiet AGNs are strong X-ray emitters and are considered as possible sources of UHECR and high-energy neutrinos. A particularly interesting group of objects is the class of blazars showing relativistic jets almost aligned with respect to the line of sight of the observer. Indeed, the peculiar orientation

([2]) For a clear review see [108].

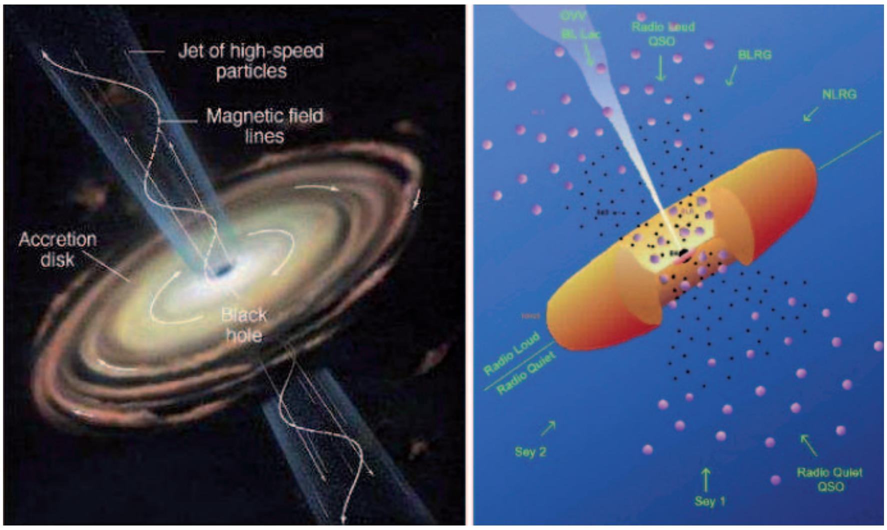

Fig. 14. – Left: Pictorial view of an AGN with its basic morphological features. Right: The astronomical classification of AGNs is based on the orientation of the AGN with respect to the observer's angle of sight on the Earth.

of the blazars and the strongly enhanced flux of the Doppler boosted radiation allow to perform detailed multi-wavelength investigations of these objects. Several blazars have been recently observed in gamma TeV [56] and they are indeed the most numerous extra galactic objects observed in these wavelengths.

The most distant observed source, 3C279 [110, 111], was detected by the MAGIC telescopes at red-shift $z = 0.538$ that is a value close to the VHE gamma horizon. However, as previously discussed, VHE gamma energy spectra observed at the Earth are distorted by the interaction with the EBL that produces both a reduction of the VHE gamma flux and a softening of their energy spectra that become more and more relevant with increasing distances.

Hadronic acceleration mechanisms were proposed to describe the observed AGN emissions [112], in this case a neutrino signal correlated to the TeV gamma-rays is expected. Different hypotheses on the details of the acceleration mechanisms in AGNs, lead to different models and to fluxes that vary by substantial factors. Neutrinos can be produced by UHE proton beam dump close to the AGN core (a region optically thick both to CR and gamma-rays), inside the AGN jet from protons accelerated by internal shocks or close to the radio lobes, at the end point of the jets [113, 114]. However, the question about the origin of the VHE gamma emission observed in blazars, namely leptonic or hadronic is still open.

In fig. 46 in the "Conclusions" we show the expected cumulative energy spectra of ν evaluated for several AGN classes on the basis of average population numbers and observed electromagnetic fluxes. Blazar models, describing proton acceleration in the jet, foresee neutrino spectra peaked at high neutrino energy ($E \simeq 10^8$ GeV). However the most optimistic models, such as the one proposed by Stecker and Salamon [115], were already disconfirmed by the AMANDA detector [116] (see subsect. **8**˙2) and recently revised [117]. A deeper discussion of the various models and of neutrino fluxes can be found in [106].

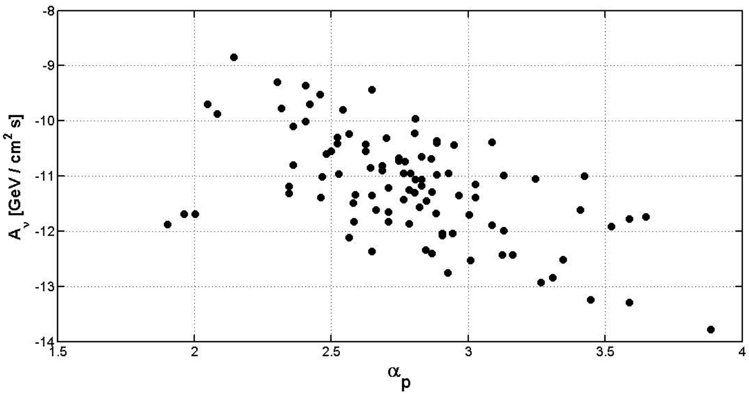

Fig. 15. – Correlation between the expected neutrino flux normalization factor and the primary proton spectral index α_p for FR-II and FSRQ radio galaxies. Most of the sources exhibit a flux $A_\nu \leq 10^{-11}$ and a correlation between A_ν and α_p is observed — brighter sources show a harder spectrum [106].

Since for several AGNs, a strong time variability is observed in gamma TeV emission, the occurrence of flares can be exploited to enhance the possibility of detection from singles or stacking AGNs in high-energy neutrino telescopes but using temporal cuts beside spatial cuts.

In ref. [106] a list of AGNs, TeV γ emitters, candidate for neutrino stacking search is reported together with the expected neutrino fluxes. In the same paper, possible correlation between the radio emission of FR-II galaxies (Fanaroff and Riley, Class II [109]) and FSRQs (Flat Spectrum Radio Quasars) and proton acceleration is exploited. In fig. 15 we report the correlation between expected neutrino fluxes and proton spectral indexes $\alpha_p = 2 \cdot \alpha_{radio} + 1$: the harder the spectrum the the higher the expected neutrino flux.

A very interesting radio galaxy is Centaurus A (Cen A), our nearest AGN, shown in fig. 16. As discussed in sect. **2**, a possible correlation between Cen A and the arrival directions of a few high-energy events detected in the Pierre Auger Observatory has been suggested. Moreover, recent VHE gamma observations of Cen A made by HESS [118] exhibit emission features compatible with a hadronic acceleration mechanism parameters.

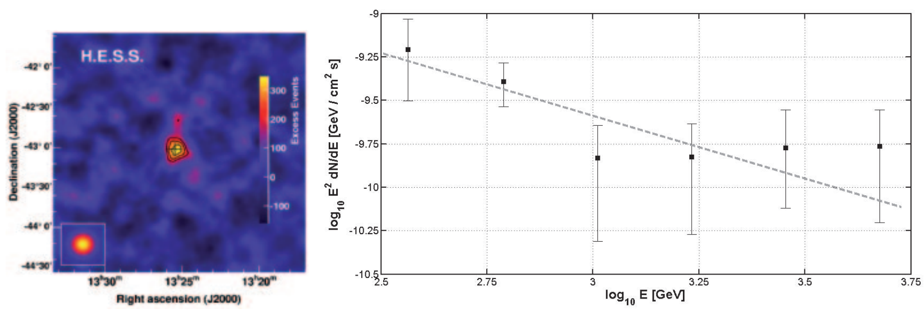

Fig. 16. – The Centaurus-A Galaxy observed by HESS in gamma rays. Left: Image of the source. Right: The measured differential photon spectrum [118].

Another very important piece of information was provided by the recent observations of the M87 radio galaxy by joint measurements in radio and VHE gamma [119] revealed a period of strong VHE gamma flares in coincidence with a strong enhancement of the radio emission from the core. These results imply the acceleration of charged particles up to very high energy in the proximity of the central black hole, but still do not permit disentangling between leptonic and hadronic origin of the VHE gamma emission.

5˙2. *Gamma-Ray Burst.* – Gamma-Ray Bursts (GRB) are among the most mysterious and violent phenomena ever observed in the Universe. A comprehensive review is reported in ref. [120], in the following only the basic features and their possible association with high-energy neutrino emission are discussed. The total energy release of GRBs is huge ($\geq 10^{51}$ erg) though they are transient sources: their emission in hard-X-ray and soft-gamma photons lasting from millisecond to several hundreds of seconds, with a late afterglow in IR, radio and optical band. Historically, gamma-ray bursts were discovered as extremely intense gamma-ray flashes in 1967 by the Vela satellites [121], launched by the U.S. to monitor the sky for nuclear explosions that might violate the Nuclear Test Ban Treaty. It was soon realized that GRB distribution in the sky is almost isotropic, thus suggesting an extragalactic origin, and their emission has been measured over a very broad interval of wavelength. A major step was provided in the late 90's by the Beppo-SAX satellite [122] measurement of the X-ray afterglow that permitted to localize the GRB and to send an alert to ground-based optical telescopes that succeed in identifying the host galaxy and determining its redshift, thus providing a conclusive evidence of the fact that GRB are at cosmological distances. A subsequent important step was achieved through the HETE-2 satellite [123] that, beside many other interesting observations, localized GRB 030329 that was the first GRB unambiguous associated with a supernova explosion [124, 125]. The launch of the SWIFT satellite [126] in November 2004 lead to further remarkable advances in the field revealing the unexplored afterglow behavior lasting from minutes to hours, as well as the afterglow of so-called "short" gamma-ray bursts (gamma emission briefer than 2 s, described in the following) and extending the gamma-ray burst observations beyond $z = 6$ in redshift where very few astrophysical objects have been ever measured. The last frontier of GRB detection was achieved with the launch of FERMI satellite [127] in June 2008 that largely extends the observability of GRB at energy higher than 100 MeV detecting almost 250 burst/year.

However, in spite of a large numbers of GBRs observed since their discovery and of the fact that their emission features have been studied in details, the nature of these objects remains mysterious to a large extent. The bulk of the emission features indicate a non-thermal process, driven by a catastrophic event involving charged particle acceleration and the conversion of huge quantities of matter into energy. Accordingly to the duration of their γ emission a bimodal time distribution of GRBs is observed: for emission times $t \geq 2$ s they are named "long" GRBs, while for $t \leq 2$ s they are named "short" GRBs. These two classes of observations seem to be associated to different progenitors: the core collapse of a massive star appears as a convincing explanation for long GRB, while compact merger of neutron star-neutron star (NS-NS) or black hole-neutron star (BH-NS) is the proposed scenario for short burst.

Concerning the photon fluence, energy releases up to $\Omega_\gamma/(4\pi) \times 10^{54}$ erg — where Ω_γ is the angle into which the gamma emission is beamed — are observed.

The hypothesis of emission from a jet, similarly to AGN, allows to accommodate the huge *gamma*-ray fluence with the extremely large distances, deduced by redshift measurements.

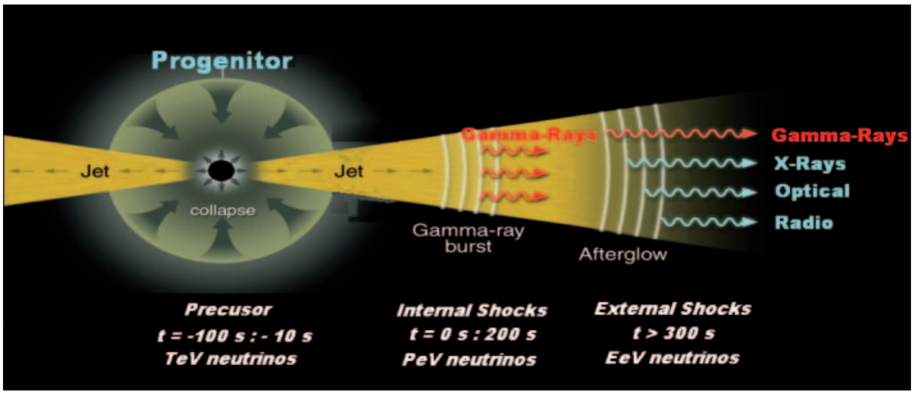

Fig. 17. – The standard scenario for GRBs. Neutrino fluxes are emitted in different stages of the jet propagation: inside the progenitor shell (precursor), in the jet internal shocks (fireball) and in the jet external shocks (afterglow).

The leading model for the electromagnetic radiation from GRBs assumes that in the catastrophic event due to collapse or merger into a black hole, surrounded by rapidly accreting masses, a fireball is created and expands at highly relativistic velocity with a large Lorenz factor ($\Gamma = 300$ being a typical value). The non-thermal features that dominate the γ-ray spectrum are therefore due to charged-particle interaction with the shock waves created as a consequence of the fireball expansion. On the basis of energetics and dynamical considerations, Waxman proposed a scenario where highest cosmic rays ($E \geq 10^{20}$ eV) are produced by GRBs [128] via a Fermi mechanism occurring in internal shocks.

GRBs are expected to emit neutrinos during several stages of their evolution: first of all, although never observed, quite a large fraction of the whole energy released is expected to be carried out by neutrinos (at 1–10 MeV energy) and gravitational waves in first stages following the collapse. A "precursor" TeV neutrino flux, without gamma counterpart —due large optical depth of the medium—, is expected about 100 s before the gamma flash, that is seen only when the jet outcomes the external progenitor shells [129]. Then, hadron acceleration in both internal shocks (jet) and external shocks (afterglow) would lead to high energy neutrino production due to p-p or p-γ interaction, as shown in fig. 17.

Accordingly to the various stages in which high-energy neutrinos are produced and to the jet feature, different energy spectra are expected. The neutrino energy spectrum in the internal shock phase depends on the jet Lorentz factor. In fig. 46 we report the muon neutrino spectrum expected from a GBR with $\Gamma = 300$ and $z \simeq 2$ [106]. While the diffuse emission from the bulk of GRBs is expected to be in the sensitivity domain of km^3-scale telescopes, the possibility of detecting neutrinos from a single burst strongly depends on burst features, such as its fluence, redshift and Γ Lorentz factor. However a "staking source" analysis on several bursts seems to be very promising. In fact GRB neutrino detection is almost background free, triggered by satellite alerts, that allow to tune the search for neutrino signals from the burst direction in a time window around the γ burst.

A GRB analysis was presented by the IceCube Collaboration [130] (see subsect. **8**˙3). At difference with other VHE gamma sources, the estimate of high-energy neutrino flux search from GRBs cannot be constrained from experimental data from TeV gamma telescopes. Indeed, in spite of very extended campaigns with several different instruments no positive observation was made so far in these high energies [131-133]. The absence of observation is expected to be mainly due to the distance of the observed GRBs that are peaked at rather high redshift, while the cosmological γ-ray horizon is at $z \simeq 1$ at $E_\gamma = 70\,\mathrm{GeV}$ and much closer at higher E_γ (see fig. 1).

5˙3. *Starburst galaxies.* – Starburst galaxies are regions where an exceptionally high rate of star formation is observed mainly by means of their radio emission. The high rate of SurperNova explosions expected in these regions would enrich the ambient gas with highly relativistic electrons and protons that interact with the interstellar medium. In the case of protons the interaction would lead to pion production and therefore to a neutrino flux. Loeb and Waxman suggested that starburst galaxies are potential sources of high-energy neutrinos and calculated a cumulative flux of $E_\nu \Phi_\nu = 2 \cdot 10^{-8\pm0.5}\,\mathrm{GeV\,cm^{-2}\,s^{-1}\,sr^{-1}}$ [134], that is in the range of detectability of a km^3-size detector. The very recent measurement by Veritas of VHE gamma from the starburst Galaxy M82, the closest of these objects in the Northern Hemisphere [135,136] represents the first observation of an extragalactic VHE gamma source not belonging to the AGN class and could provide very interesting information about these cosmic objects. Moreover, limits on the closest starburst galaxy on the other hemisphere, NGC 253, have been set [137].

5˙4. *Cosmogenic neutrinos.* – As discussed above, the interaction of UHE protons ($E_p \geq 10^{19}$) eV with the CMBR via the Δ-resonance (energy threshold $E \simeq 5 \cdot 10^{19}\,\mathrm{eV}$) leads to the prediction of the GZK cut-off in the UHECR energy spectrum.

The range of UHE proton propagation in the Universe, associated to the $p\gamma \to \Delta(1232\,\mathrm{MeV})$ resonance channel, is expected to be as low as few tens Mpc.

A natural consequence of the GZK cut-off will be the existence of flux of ultra-high-energy cosmogenic (or GZK, or BZ) neutrinos produced by the decay of charged pions, resulting from $\Delta \to N\pi$ decay [138]. The diffuse flux of BZ neutrinos is considered, to some extent, a "guaranteed" neutrino flux.

The energy spectrum of GZK neutrinos is expected to span the range between approximately $E \geq 10^{16}\,\mathrm{eV}$ and $E \leq 10^{21}\,\mathrm{eV}$, while the shape and flux depend on several factors such as the primary UHECR flux spectral index and composition. This lead to predictions from different models that show remarkable variations on GZK neutrino fluxes as shown in fig. 46 [139-141].

On the other hand the recent results by Auger —although they provide a further confirmation of the UHECR flux suppression observed already by HIRES— show a spectral shape at UHE different from the one measured by HIRES and fit with a nuclear mass composition that becomes heavier with increasing energy (as described in sect. **2**). This is in contrast with HIRES results that show a proton dominance also at the highest energy. Many different interpretations, aiming at understanding these discrepancies, are proposed in order to clarify the nature of the suppression observed in the UHECR spectrum [142].

A possible consequence of the scenario in which the CR flux is dominated by heavier nuclei at extreme energy, is that the observed CR flux reduction is only due to limited —intrinsic— acceleration power of the astrophysical sources. In this latter case, the absence of a GZK cutoff would reflect into absence of cosmogenic neutrinos.

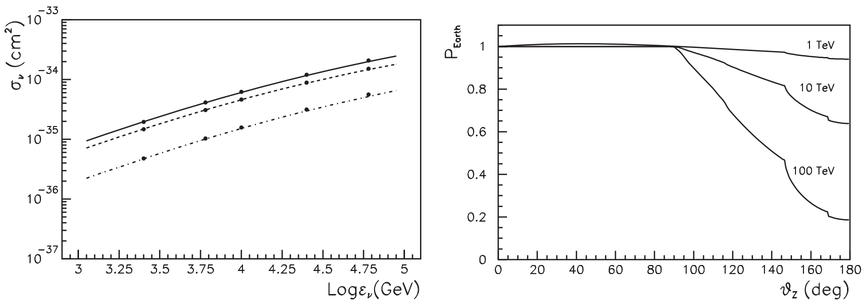

Fig. 18. – Left: The neutrino-nucleon cross-section as a function of energy for charged-current interaction (dashed line), neutral-current (dotted line) and total cross-section (solid line). Right: Neutrino absorption probability in the Earth as a function of the zenith angle for $E_\nu = 1\,\text{TeV}$, $10\,\text{TeV}$ and $100\,\text{TeV}$, respectively.

6. – High-energy neutrino detection

As shown in the previous section, light and neutral neutrinos are optimal probes for high-energy astronomy, *i.e.* for the identification of astrophysical sources of UHE particles [143]. To fulfill this task neutrino detectors must be design to reconstruct both the neutrino energy and direction, thus they are commonly referred as *Neutrino Telescopes* (for a clear review see [144]).

At energies above few hundreds GeV, neutrinos are detected through deep-inelastic scattering of the ν with a target nucleon N. In the $\nu + N \rightarrow l + X$ interaction, the lepton l escapes while the hadronic debris X leads to a hadronic cascade. The initial neutrino energy E_ν, is shared among the lepton E_l and the hadronic cascade. The cascade carries $E_h = y \cdot E_\nu$, where y is the Bjorken inelasticity parameter, with a mean value of $\langle y \rangle \simeq 0.25$ at very high energies, and a very broad distribution; the lepton takes the remaining energy [145].

In weak charged-current (CC) interactions the outgoing lepton is charged and it preserves the neutrino flavour (e, μ or τ). In neutral-current (NC) interactions, the outgoing lepton is a neutrino, thus only the hadronic cascade is detectable.

The detection of the ν interaction is, therefore, based on the observation of the outgoing charged lepton and/or of the hadronic cascade.

The νN cross-section is as low as $\sigma_{\nu N} \simeq 10^{-35}\,\text{cm}^2$, at $\simeq 1\,\text{TeV}$, increasing linearly with the neutrino energy up to 5 TeV energy, above this value its slope changes to $E^{-0.4}$, as shown in fig. 18 [146]. The increase of the neutrino cross-section as a function of energy implies also that at $E > 10\,\text{TeV}$, the Earth is not transparent to neutrinos. Figure 18 shows the probability of absorption of neutrinos as a function of zenith angle for different neutrino energies, taking into account the different densities of the Earth core, mantle and crust [147]. This effect plays an important role for the energy range accessible to different experimental techniques, as described in the following.

Due to the low νN cross-section and to the faint expected astrophysical ν fluxes ($\propto E_\nu^{-2}$), the detectors must have a ν interaction target mass of several GTons for $E_\nu \simeq 10^{12}$–10^{17} eV and much larger for higher energies. For this reasons Markov, Zheleznykh and Askaryan proposed the use of natural media to detect cosmic neutrinos [148].

Depending on the candidate interaction target medium and on the energy range to explore, different experimental techniques were proposed (see fig. 19):

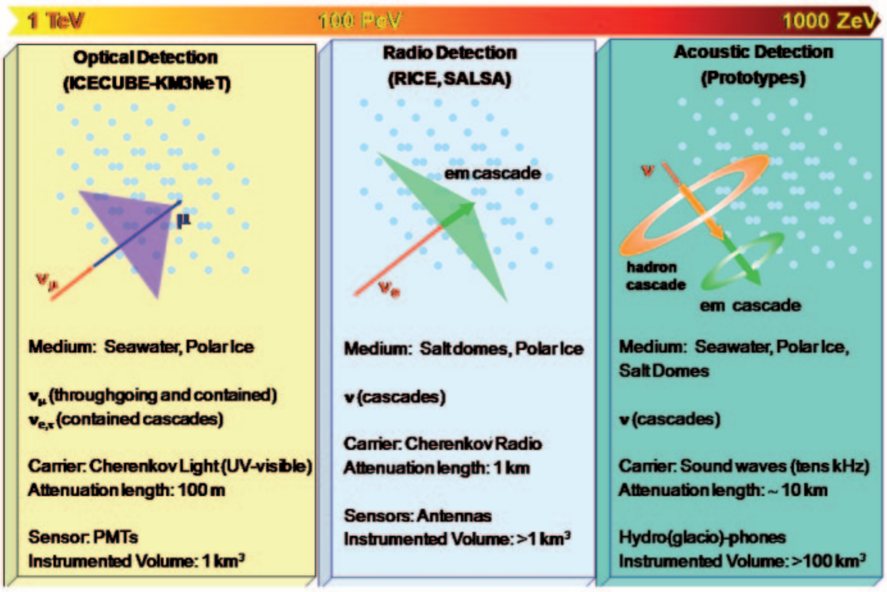

Fig. 19. – Detection techniques for high-energy astrophysical neutrinos as a function of the ν energy range.

– in the range $E_\nu \simeq 10^{11}\,\text{eV}$–$10^{17}\,\text{eV}$, the technique is based on the detection Čerenkov light originated by charged leptons outgoing a CC neutrino interaction in seawater or in the polar ice-cap [148];

– at higher ν energies, the proposed experiments rely on: the detection of radio pulses produced by e.m. showers following a neutrino interaction in polar ice, salt domes or in the Moon regolith [149, 150]; the detection of acoustic waves produced by deposition of energy in the interaction of ν in seawater, polar ice-cap or salt domes [151]; the detection of air showers initiated by neutrinos interacting with rocks or deep Earth's atmosphere [152].

In the following sections a more detailed description of the different techniques is given together with a closer view on the status of experiments.

7. – Underwater/ice Čerenkov technique

Among all, the underwater/ice Čerenkov technique is, at present, the most promising and advanced. The idea, proposed by Markov [148], is based on instrumentation of large volumes of sea/lake water or polar ice, in order to detect the charged leptons (in particular muons, as we will discuss) emerging from a CC neutrino interaction. Underwater(ice) Čerenkov neutrino detectors are large arrays of optical sensors, typically photomultiplier tubes (PMTs) of about $10''$ diameter, which permit charged leptons tracking, by timing the Čerenkov light wavefront radiated by these particle.

In water and ice, relativistic particles radiate Čerenkov light mainly in the UV-blue wavelengths. In both media the refractive index in this spectral region is $n \simeq 1.35$, and photons are emitted the along particle track at the angle $\vartheta \simeq 42°$ and symmetrically in

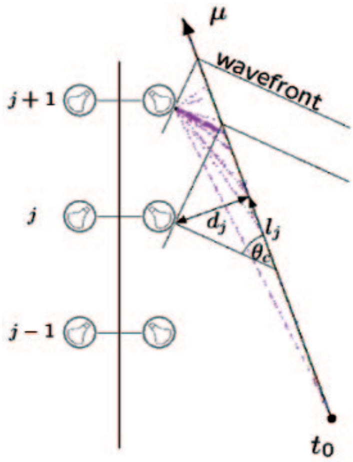

Fig. 20. – The lepton Čerenkov wave front is reconstructed using the information on photon hit and PMT positions (see eq. (6)).

phi. The time sequence of Čerenkov photons hits on PMTs is thus correlated by the space-time causality relation (see fig. 20):

$$c(t_j - t_0) = l_j + d_j \tan(\vartheta_{\check{C}}). \tag{6}$$

The above relation is used to reconstruct the Čerenkov wave front, therefore the particle track, from the experimental data. The reconstructed track direction is however affected by experimental indetermination: the error on PMTs position and on absolute photon hit time, due to photon scattering in the medium, PMT transit time spread and to detector time calibration. Photon scattering in the medium is an important issue, since scattering deflects Čerenkov photons, affecting track direction reconstruction. In ice the scattering length of light is only few tens of cm, in water it is about 100 m [153].

It is worth mentioning that particle energy loss via Čerenkov radiation is only a small fraction of the total one, and the number of Čerenkov photons (UV-blue) is only 300 per cm of track. Given this small amount of light, photons hits PMTs only if the average distance between optical sensors is not larger than the light absorption length in the medium. The medium optical properties, thus, determine the detector granularity (*i.e.* the PMT density) and its size. As shown in fig. 21, water is transparent only to a narrow range of wavelengths (350 nm $\leq \lambda \leq$ 550 nm). In particular, for deep polar ice L_a(UV-blue nm)$\simeq$ 100 m [154], and it is about 70 m for clear ocean waters [153]. This leads to the use of not less than $\simeq$ 5000 optical sensors per km^3.

The "golden channel" for astrophysical neutrino detection is the ν_μ CC interaction. The muon range in water is, at $E \simeq$ TeV, of the order of kilometres (see fig. 22), therefore the ν_μ interaction can take place either within the detector or far outside it, providing a flux of high-energy muons, either contained or crossing the detector. The muon direction is recovered from the reconstruction of the Čerenkov wave front, radiated along the muon track, within the detector instrumented volume. The detection of the neutrino-induced muon also allows "neutrino astronomy": the angle between the outgoing muon and the interacting neutrino decreases as a function of neutrino energy (see fig. 22): at

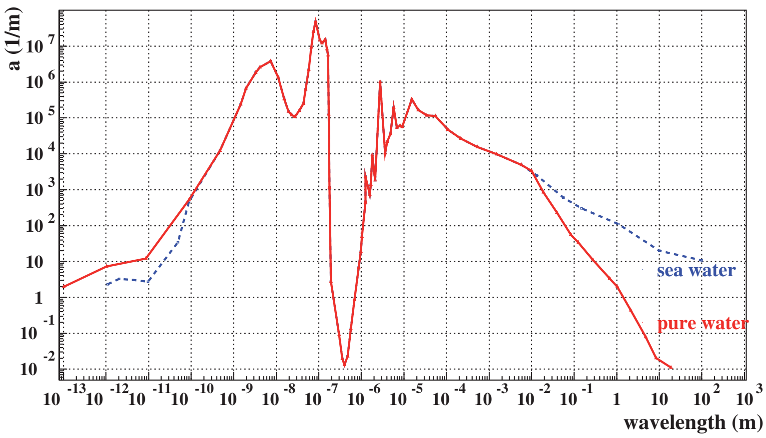

Fig. 21. – Light absorptionas a function of wavelength for pure water (solid line) and seawater (dashed line). The absorption length is defined as $L_a(\lambda) = a^{-1}(\lambda)$.

$E_\nu > 1\,\text{TeV}$, the muon track is almost co-linear to the ν_μ one and permit pointing back to the ν cosmic source. These detectors are, in fact, also named as *Neutrino Telescopes*.

For the muon neutrino detection, up-going or horizontal muon tracks are preferred. In fact, when an upward-going muon is reconstructed this is a unique signature of a neutrino event, being the up-going atmospheric muon background completely filtered out within few tens of km of water (see fig. 23). The suppression of the intense down-going atmospheric muon flux is achieved installing the detector at large water(ice) depth: the muon stopping power of 3000 m of water is equivalent to the one of 1 km of rock. Water and ice have, therefore, a threefold function: huge (and inexpensive) neutrino target, Čerenkov light radiator and shield for cosmic muon background.

Neutrino telescopes are also expected to disentangle between neutrino flavours by reconstructing the Čerenkov wave front shape of the event which depends on the different propagation of e, μ and τ in water (and ice).

In case of ν_e CC interactions, the final state involves high-energy electrons that provide a high-energy electromagnetic shower superimposed on the hadronic one. Both showers extend for few tens of metres from the ν interaction point, thus only interactions that

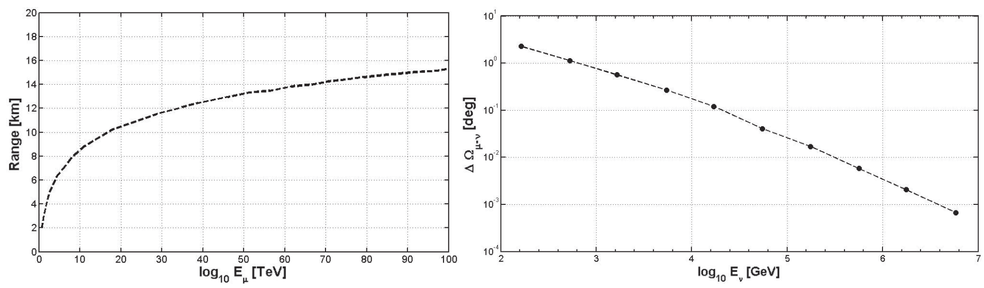

Fig. 22. – Left: Average muon range in water as a function of muon energy. Right: Median of the distribution $\Delta\Omega_{\nu-\nu_\mu}$ (muon exit angle with respect to the ν_μ direction) as a function of neutrino energy.

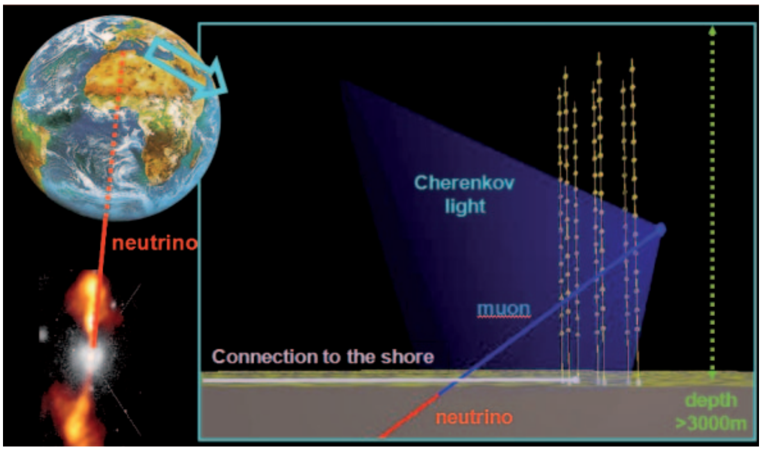

Fig. 23. – Detection principle of an underwater neutrino telescope: Astrophysical neutrinos reach the Earth and interact in water or close to the seabed generating a muon. The array of several thousands optical sensors detect Čerenkov photons generated along the muon track. A water shielding $\geq 3000\,\mathrm{m}$ reduces the atmospheric μ flux by a factor $\simeq 10^6$ with respect to sea surface.

are fully contained into the detector instrumented volume, or very close to it, can be identified. At distance of few hundreds metres from the shower, the shape of the light wavefront is similar to an expanding sphere, thus, the neutrino direction is difficult to reconstruct. On the other hand, showers involve a large number of charged particles ($N \propto E_\nu$) radiating Čerenkov light and, in this case, the lepton energy can be well estimated from the shower light yield. Photon yield is also effectively used to estimate energy in UHE ν_μ detection, for which the muon generates high-energy showers along its path([3]). The charge dynamic range of the PMTs and their readout electronics is therefore an important parameter. The scenario depicted for ν_e is similar to the case of tau-neutrino detection: up to $E_\nu \simeq 1\,\mathrm{PeV}$ the τ decay length is too short ($\simeq 50/E_\tau\,\mathrm{mm/TeV}$) to reconstruct the τ decay shower from the hadronic one. When the τ path is about 100 m long, then, the two cascades can be separated and the event topology shows the typical signature of a "double light bang".

In order to calculate the number of detectable events expected by cosmic-neutrino fluxes it is important to introduce the quantity $P_{\nu\mu}$, which is the probability to convert neutrinos into detectable muons. $P_{\nu\mu}$ is a function of the neutrino interaction cross-section and of the average muon range $R(E_\mu, E_\mu^{min})$:

$$P_{\nu\mu}(E_\nu) = N_A \int_{E_\mu^{min}}^{E_\nu} \mathrm{d}E\mu \frac{\mathrm{d}\sigma_{\nu N}^{CC}}{\mathrm{d}E\mu} R(E_\mu), \tag{7}$$

where N_A is the Avogadro number and E_μ^{min} is the minimum detectable muon energy, or detector threshold. For a given detector the value of $P_{\nu\mu}$ has to be calculated via

([3]) For low-energy "naked muons", the indetermination of the reconstructed energy is large, indeed, since the number of Čerenkov light photons is small.

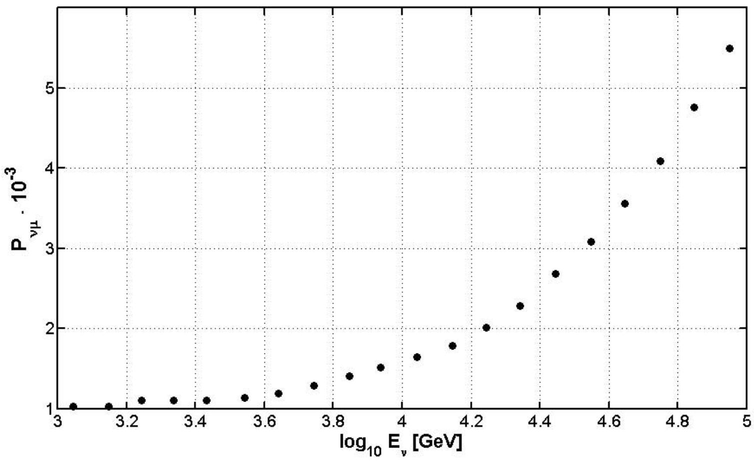

Fig. 24. – The $P_{\nu\mu}$ as a function of neutrino energy for different detector thresholds: 1 GeV (triangles) and 1 TeV (circles). The line represents the parametrization of Gaisser [144] for 1 GeV threshold.

simulations [144]. As a rule of thumb $P_{\nu\mu} \simeq 1.3\times10^{-6}$ for TeV neutrinos ($E_\mu^{min} = 1\,\text{GeV}$) and it increases with energy([4]) as $E^{0.8}$, as shown in fig. 24.

As already mentioned, above 10^{12} eV, the muon range is larger than several kilometres, and detectable muons can be originated far from the detector sensitive volume. The parameter usually quoted to describe detector performance for muon neutrino detection is its *effective area* — A_{eff} for muons, *i.e.* the surface intersecting the neutrino-induced muon flux folded with the detection efficiency for muons. The rate of events produced by a neutrino flux $\Phi_\nu(E_\nu, \vartheta)$ per unit of detector effective area, is then expressed by

$$\frac{N_\mu(E_\mu^{min}, \vartheta)}{A_{eff}\ T} = \int_{E_\mu^{min}}^{E_\nu} \mathrm{d}E_\nu \Phi_\nu(E_\nu, \vartheta) P_{\nu\mu} e^{-\frac{Z(\vartheta)}{L_{\nu N}(E_\nu)}}, \tag{8}$$

being $L_{\nu N}$ the neutrino absorption length in the Earth and $Z(\vartheta)$ the Earth column depth (see fig. 18).

Plugging the WB bound flux (see formula (5)) into eq. (8) and integrating over the solid angle, one gets a rate of about 10^2 up-going events per year for a 1 km^2 effective area detector with $E_\mu \simeq 1\,\text{TeV}$ threshold. This number set the scale of dimension for astrophysical neutrino detectors.

Due to photon detector and installation costs, the affordable size of these apparatuses is of the order of few km^3. This size is optimal for the exploration of the ν energy range 10^{11} eV–10^{17} eV.

The study of detector performance in details requires Monte Carlo simulations that have to take into account the detector layout, the characteristics of the Čerenkov radiator which surrounds the detector (light refraction index, light absorption and scattering coefficients) and the sources of background, that will be discussed in the following section.

([4]) For $E_\nu \gg E_\mu^{min}$ the $P_{\nu\mu}$ shape is independent of E_μ^{min}.

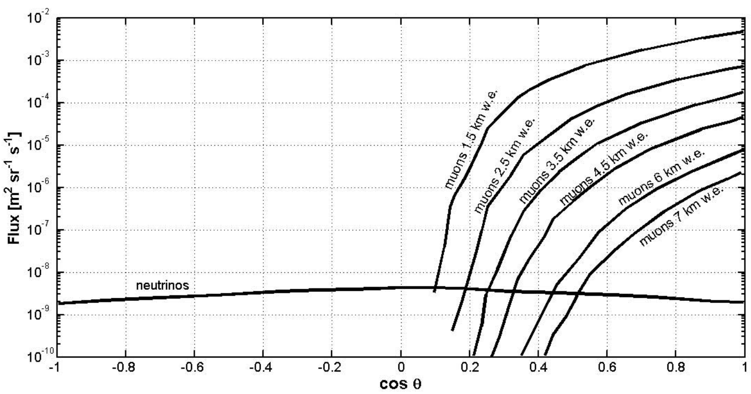

Fig. 25. – Atmospheric muon and neutrino fluxes as a function of zenith angle for different depths of installation of a detector in units of metres of water equivalent (m.w.e.).

Simulations show that an underwater detector having an instrumented volume of about $1\,\text{km}^3$ equipped with several thousands of optical modules can achieve an affective area of $\simeq 1\,\text{km}^2$ and an angular resolution of $\simeq 0.1°$ for $E_\mu > 10\,\text{TeV}$ [155].

7·1. *Sources of background.* – There are different kinds of backgrounds with which optical Čerenkov neutrino telescopes have to cope: atmospheric μ and ν background and optical background that affects only underwater telescopes. In neutrino detectors a few cosmic neutrino events have to be identified and sorted among a huge diffuse atmospheric background. Atmospheric muons (produced by the interaction of primary cosmic-rays with the atmosphere) that at sea surface exceed the number of neutrino-induced up-going muons by about 10 orders of magnitude, are attenuated in flux and energy below the sea surface as a function of depth and as a function of zenith angle: it falls to zero near the horizon and below where the large slant of water and the Earth shield all the muons (fig. 25). This is the reason why astrophysical neutrino signals are (mainly) searched among upward-going muons. Since at 3000 m depth, an underwater neutrino telescope "sees" a cosmic muon flux still about 10^6 times higher than the up-going atmospheric neutrino signal, accurate reconstruction procedures and quality cuts are needed to get rid of the atmospheric muon tracks mis-reconstructed as "fake" up-going. The atmospheric neutrinos are instead an unavoidable source of background and only energy cuts and statistical arguments allow to discriminate these events from astrophysical ones during data analysis. In fact, atmospheric ν flux is expected to produce diffuse events with a known spectral index ($\alpha \simeq -3.7$ at $E_\nu > 10\,\text{TeV}$) [156] while neutrino fluxes coming from astrophysical point sources are expected to follow an E^{-2} and to be concentrated within a narrow angular region, in the direction of their source, whose dimension is essentially given by the detector angular resolution. Diffuse flux searches look for an excess of signals above the atmospheric neutrino flux for a given energy threshold (about 10^5 GeV) and in this case the major concern is the poor knowledge of the component due to the prompt charm decay. Both atmospheric muons and neutrinos are besides sources of background as discussed above, very useful sources of calibration. In particular, atmospheric muons can be used to verify the pointing accuracy of the neutrino telescope and its absolute positioning by detecting the Moon shadow. This method, already exploited by the MACRO [157] and ARGO [158] experiments, is currently used also by the

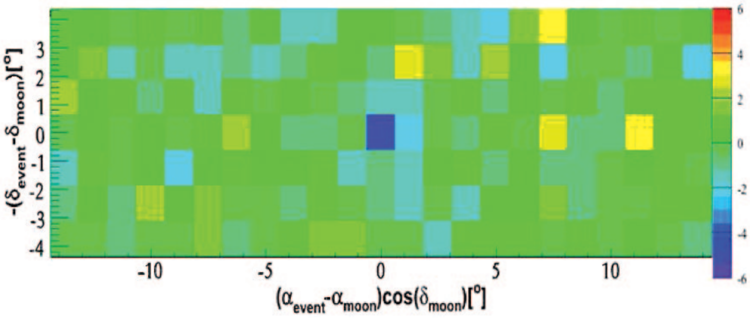

Fig. 26. – Observation of the Moon shadow effect in the cosmic muon flux with IceCube. The color scale refers to the significance of the atmospheric muon flux deficit in the Moon direction. Data show a 5σ significance.

IceCube Collaboration (see subsect. **8**˙3) that presented the first preliminary results on the muon deficit from the Moon direction, shown in fig. 26 [159]. On the other hand, the measurement of the the atmospheric neutrino energy spectrum is of crucial importance since it allows to calibrate the detector and in the near future it will provide data in the region of the prompt charm decay where theoretical expectations vary a lot.

A different source of background is the optical noise in seawater that superimposes random hits that are not correlated to the track to the hits produced from charged leptons. This background is due to the presence of radioactive isotopes and bioluminescent organisms. Radioactive elements in seawater (mainly ^{40}K contained in salt) emit electrons above the Čerenkov threshold. The uncorrelated background produced by ^{40}K decay on PMTs was measured to be about few tens of kHz for $10''$ PMT (at 0.5 single photoelectron —s.p.e.— threshold) [155] and does not depend on the site since the salt concentration variations are negligible. Optical noise is also due to bioluminescent organisms living in deep water. These organisms (from small bacteria to fish) produce long-lasting ($\simeq 10^{-3}$ s) bursts of light that may saturate close PMTs for the period of emission. In oceanic very deep seawater, bioluminescence signals are rare (few per hour) and do not affect the average optical noise rate on PMTs, as measured at 3000 m depth in the Capo Passero site — latitude: 36° 30′, longitude: 016° 00′— and reported in fig. 27. On the contrary, in biologically active waters, bioluminescence signals may produce an

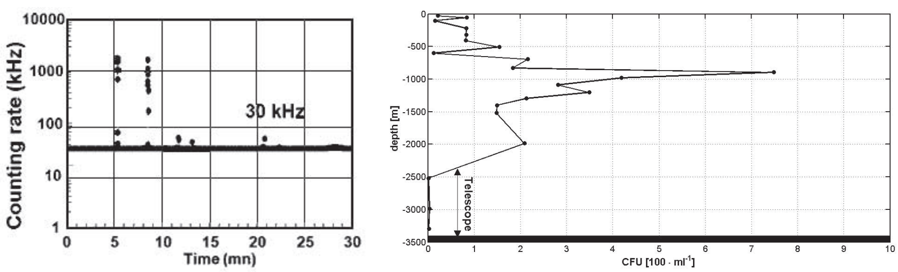

Fig. 27. – Left: Optical background rate measured at 3000 m depth in the Capo Passero site — latitude: 36° 30′, longitude: 016° 00′, Ionian-Sea plateau. Right: Concentration of bioluminescent bacteria as a function of depth measured in the same site.

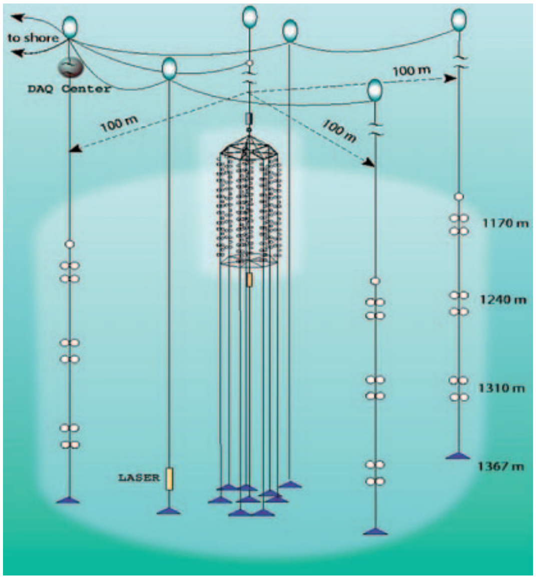

Fig. 28. – Pictorial view of the Baikal telescope NT200+: the compact NT200 detector (center) and the three outer strings are shown.

intense background noise up to several hundreds kHz (on 10″ PMTs, 0.5 s.p.e) [155]. Background hits have to be filtered by event triggers and reconstruction algorithms. Very high rates of bioluminescence can deteriorate the track reconstruction quality and in the worst cases could affect the data transmission.

8. – Status of neutrino telescope projects

The realization of km^3-scale neutrino Čerenkov detectors both under the ice and in deep water requires extended R&D activities in order to cope with the huge technological challenges that work in hostile environments (high-pressure, low-temperature, corrosion, ...) implies. In the following sections the status of experimental activities in the field is reported.

8˙1. *Baikal*. – After the pioneering experience made by the DUMAND Collaboration off-shore Hawai Island [160], Baikal was the first neutrino telescope operating underwater. The Baikal Neutrino Telescope (NT) is operated in Lake Baikal (Siberia) where the detector is moored between 1000 and 1100 m depth [161]. Deployment and recovery operations are carried out during winter, when a thick ice cap of about 1 meter is formed over the lake. After a first deployment stage, in 1993 (NT36, equipped with 36 PMTs), the Baikal NT200 (fig. 28) was completed in 1998 and it takes data since then. Baikal NT200 is an umbrella-like array with a 72 m height and a diameter of 43 m. It is made of 8 strings, each with 24 pairs of down-looking Optical Modules (OM). Each OM contains a 37 cm quasar photomultiplier. The two OMs of a pair operate in coincidence in order to suppress the background due to bioluminescence. Baikal NT200 is a high-granularity detector with a threshold $E_\mu \simeq 15\,\mathrm{GeV}$ [162].

A rather low light transmission length in water, 15–20 m, high sedimentation, biofouling rate and a high optical background rate due to bioluminescence limit the NT200 detector performances as HE astrophysical neutrino telescope. Due also to the small lever arm, the angular resolution of NT200 for muon track is only 4°. Nevertheless, for several years, Baikal has been the largest high-energy neutrino telescope in the world and the only one operating in the Northern Hemisphere thus providing upper limits on several physics items that were the most stringent ones up to the advent of AMANDA (see subsect. **8**˙2). In particular the Baikal Collaboration set the first limits on diffuse HE neutrino fluxes. From the analysis of the 5-year sample (1008 days live time) 372 upward-going neutrino candidates were selected in good agreement with Monte Carlo simulations of atmospheric neutrinos that give 385 neutrino events to be detected in a corresponding lifetime. The collaboration has presented also data analysis of ν_e events, which set an upper limit for diffuse astrophysical neutrino fluxes $E_\nu^2\Phi_\nu < 8.1 \cdot 10^{-7}\,\mathrm{cm}^{-2}\,\mathrm{s}^{-1}\,\mathrm{sr}^{-1}\,\mathrm{GeV}$ (at 90% confidence level, not including systematic uncertainties) [162].

In order to improve the pattern recognition and vertex reconstruction of high-energy cascade events, an upgrading of the NT200 telescope, named NT200+, was realized in 2005 by adding three outer strings (see fig. 28). Each string of NT200+ is made of 12 OM each with a larger spacing. NT200+ has an enclosed detector volume of about 5 Mton and it is expected to increase the sensitivity to diffuse fluxes by almost a factor four. The collaboration also plans the construction of a km^3-size detector in Lake Baikal, the Giant Volume Detector (GVD). The GVD will be made of 90–100 sparsely instrumented strings with 12–16 OMs/string arranged over a 350 m string length. The detector will be made of triangular detection units made of three (200 m)-spaced strings and a fourth one located in the center of the triangle. GVD configuration will instrument a volume of about 0.7 km^3 for cascade ($E \geq 100\,\mathrm{TeV}$) and will detect muon with an energy threshold of few tens of TeV. NT200+ represents, in this framework, the first step towards GVD.

8˙2. *AMANDA*. – The Antarctic Muon And Neutrino Detector Array (AMANDA), constructed at the Amundsen-Scott South Pole Station was completed in 2001 [163]. AMANDA was a first-generation instrument that served as test bench for technologies and as prototype for the km^3-size detector IceCube. During an exploratory phase of the project in 1993-1994, four strings equipped with 20 OM each (with a 8″ PMT and analogue readout) were deployed between 800 and 1000 m. The strings were connected to surface electronics via coaxial cables. OMs were illuminated by laser light shot into diffusers placed close to the OMs, thus allowing time calibration and, from the arrival times on distant PMT, to derive the optical properties of the ice. These studies showed that at these depths the high residual concentration of air bubbles leads to a light scattering so strong that does not allow an accurate track reconstruction. For this reason, the next stage of the project AMANDA-B10, made of ten strings, was deployed at depths between 1500 m and 2000 m below the ice sheet surface where the concentration of residual bubbles was expected to be negligible [164].

The final detector configuration, AMANDA II that started in 2000 and run for seven years, consisted of 677 OMs arranged in 19 strings [165]. High-voltage power was provided to the OMs from the surface and the PMT signals were amplified and sent to the surface via electro-optical cables. Strings were arranged in concentric circles, the outermost diameter being 200 m, thus giving an instrumented volume of about 15 Mton of ice.

AMANDA II accumulated a total exposure of 3.8 years, taking into account maintenance periods and acquisition system dead time. The average rate of single photoelectron signals on PMTs (mainly dominated by housing and PMT glass impurities) and was about 400 Hz per PMT.

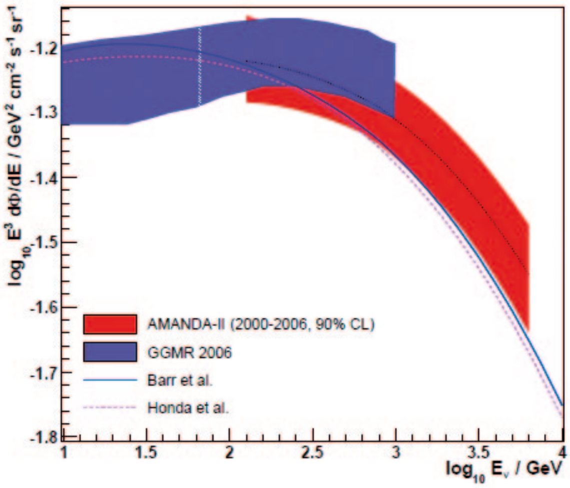

Fig. 29. – Angle-averaged atmospheric neutrino ($\nu_\mu + \bar{\nu_\mu}$) flux, measured with AMANDA, multiplied by E^3 [166]. The solid red band represent 90% Confidence Level from the forward-folding analysis. The dotted line shows the central best-fit curve. Also shown is a previous result by Gonzalez-Garcia *et al.* using Super-Kamiokande data [168], as well as Barr *et al.* [169] and Honda *et al.* [170] predictions. All fluxes are shown prior to oscillations.

The atmospheric neutrino flux, that constitutes the most relevant background to astrophysical ν searches, but also a useful calibration source, has been measured with a statistics of about 1000 events per years.

This allowed to extend the atmospheric muon-neutrino energy spectrum by several orders of magnitude compared with previous data. The neutrino energy spectrum measured by AMANDA is reported in fig. 29 together with the expected neutrino energy spectrum. The observed spectrum is consistent with the predictions, including the contribution of the so-called"prompt" atmospheric neutrinos due to the decay of charmed particles in the atmosphere, as shown in fig. 46 [166].

Despite a quite poor angular resolution (about 2 degrees), the search for astrophysical neutrino point sources was performed with an unbinned method together with a staking analysis on 26 *a priori* point-like sources. No statistically significant excess was found. The sensitivity of AMANDA for point-like sources is reported in fig. 43 at the end of this section [167].

AMANDA was incorporated into IceCube in 2007 and the detector was decommissioned in May 2009.

8·3. *IceCube.* – The experience accumulated with AMANDA both in physics and in technological issues, was fundamental for the construction of the ice-base km^3-scale detector IceCube at the South Pole. Several improvements, compared to AMANDA, were anyway necessary to undertake the IceCube construction [171]. Due to the hostile South Pole environment, which permits line deployment only in a 2 months time window over a year, the major effort of IceCube was addressed to the reduction of the time necessary to install the whole detector. The drilling method pioneered by AMANDA was made more effective by the use of a new very powerful drill with 5 MW of thermal power that allows to strongly reduce the time needed to drill a 2500 m deep, 60 cm diameter hole to about only 40 hours.

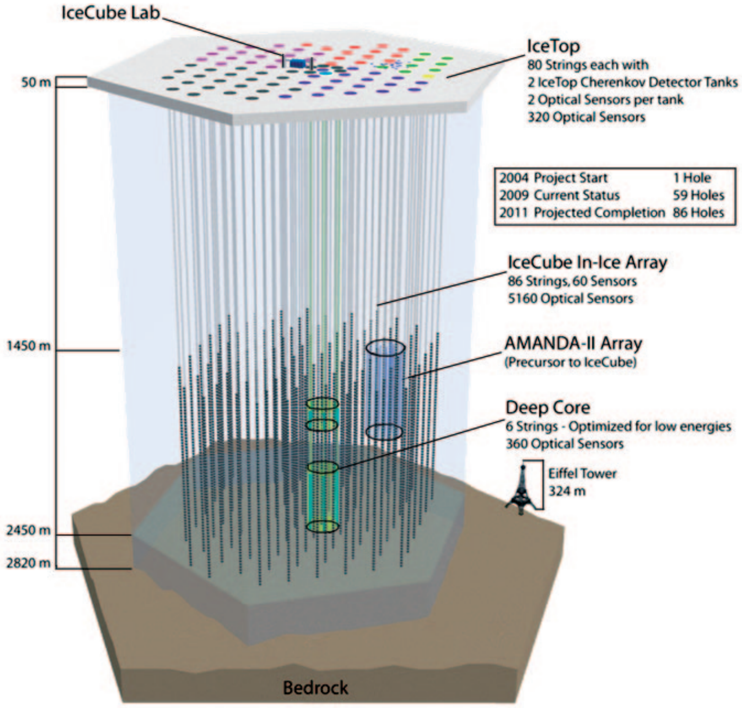

Fig. 30. – Pictorial view of the IceCube detector.

In its complete configuration, IceCube, will consists of 80 vertical strings, each equipped with 60 Digital Optical Modules (DOM) [172], deployed between 1450 m and 2450 m depth below the surface, as shown in fig. 30. The DOM spacing along the string is 17 m and the strings are placed on a hexagonal lay-out with 125 m spacing, giving 1 km^3 of instrumented volume. The DOM shown in fig. 31 contains a 10$''$ PMT and digital read-out electronics to permit signal wave form analysis, leading to a relevant improvement of the detector performance. The size of IceCube is well matched to the energy scale since a muon with an energy of about 200 GeV travels about 1 km in ice. An improvement of the telescope sensitivity in the low-energy range will be achieved by the addition of six more densely instrumented strings that will be deployed in the bottom center of the telescope to form the so-called DeepCore detector that will lower the IceCube threshold for muons to about 10 GeV, thus allowing to address more effectively low-energy physics issues and especially to increase the sensitivity for the indirect search of Dark Matter [173].

On the ice surface, above the IceCube strings, the IceTop air shower array is installed. IceTop will consist of 180 ice-filled tanks of about 1 m^3 volume, shown in fig. 31, each equipped with two DOMs [174]. IceTop allows to study high-energy cosmic-ray showers. With its 59 strings already deployed, 118 IceTop tanks in operation together with the first DeepCore line, IceCube is currently the largest neutrino telescope operating in the world.

The detector is operational since 2006: with 9 lines during year 2006 (IC9, 137 days lifetime), 22 lines (IC22, 275 days lifetime in 2007) and 40 lines (IC40, 365 days lifetime

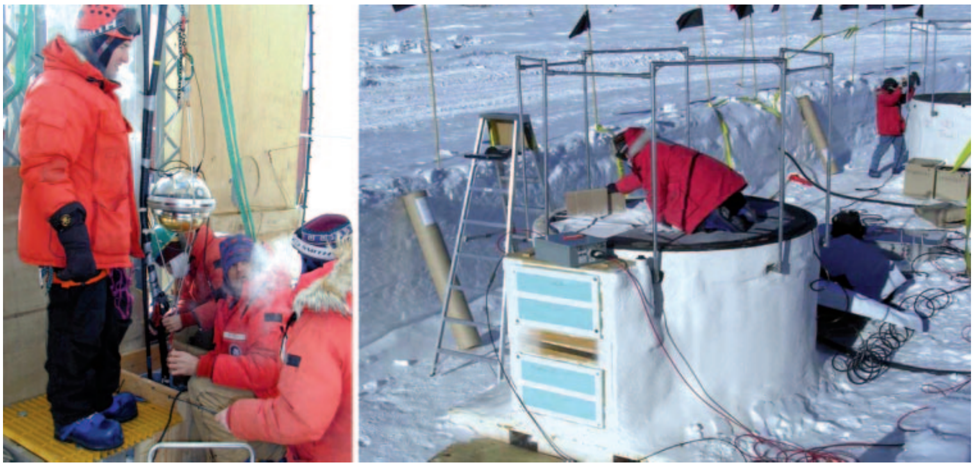

Fig. 31. – Left: Deployment of an IceCube string, equipped with DOMs. Right: A tank of IceTop.

in 2008). In the IC40 configuration the single photoelectron rate is 280 Hz per PMT, while atmospheric muon rate and muon-neutrino rate are 1000 Hz and 100 Hz of events per day, respectively. Several triggers, that use the arrival times of the hits on the DOMs, are implemented in the IceCube data acquisition software, thus allowing a first (fast) selection of events that feed a set of software filters performing a variety of simple reconstructions.

An analysis of the 275.5 day 22 string data performed with 4 different muon energy estimators gave a diffuse upper limit for a $E_{\nu_\mu}^{-2}$ spectrum of $2.5 \cdot 10^{-8}$ GeV, that does not show any excess with respect to the expected atmospheric neutrino flux, within systematics errors. Figure 46 reports the limits obtained with IC40 for diffuse muon-neutrino flux and UHE all-flavour neutrino flux, together with expectations for the complete IceCube detector (IC80) [175,176]. In the near future IceCube will be, thus, able to test the atmospheric neutrino component due to prompt charm decay and to reach a sensitivity for diffuse fluxes lower than the WB limit.

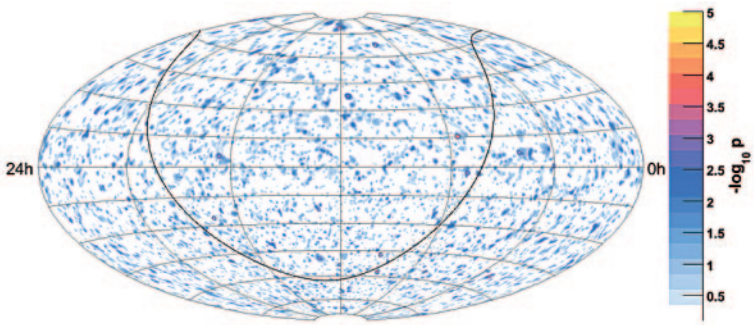

Fig. 32. – The neutrino sky map seen by Icecube.

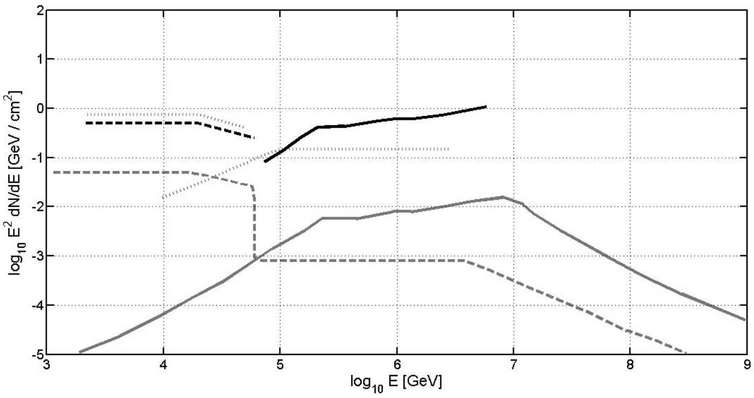

Fig. 33. – Light lines: Predicted fluences from the 41 Northern Hemisphere GRBs for different emission models: prompt (solid, sum of individual spectra) and precursor (dashed). Dark lines: 90% upper limits on the neutrino fluences obtained with the unbinned likelihood analysis [130].

Thanks to angular resolution of less than 1 degree, the sensitivity for neutrino point-like source with IC40 is strongly improved compared to AMANDA. The full neutrino sky map seen by IceCube including both up-going and down-going neutrinos is reported in fig. 32. Down-going events are selected using an energy threshold ($E_\mu \geq 10^5$ GeV) sufficiently high to get rid of atmospheric muons. No significant excess from any sky direction has been observed up to now. In fig. 43 the sensitivity to point-like neutrino sources, as a function of source declination, is reported for different stages of the project [177].

A dedicated analysis was devoted to the search for muon neutrinos from GRBs [130]. The analysis of 41 GRB, mostly detected by the SWIFT satellite [126], and the relative limits obtained with IC22 are reported, for both expected precursor and prompt emission, in fig. 33.

8˙4. *NESTOR.* – The Neutrino Extended Submarine Telescope with Oceanographic Research (NESTOR) was the first collaboration that operated in the Mediterranean Sea [178]. NESTOR indicated, for the installation of the km^3 telescope, a marine region near the Peloponnese Coast (Greece) where seabed depth ranges between 3800 m and 5000 m. As expected in the Ionian Sea (an oligotrophic environment, compared to the eutrophic Tyrrhenian Sea), recent measurements of optical and oceanographic properties in the deep waters of the site, show low optical background and light transmission length close to optically pure seawater (that is salt water without particles) [155]. On the other hand, the presence of a steep shelf break, the so-called Hellenic Trench, and of a strong seismic activity, has to be constantly monitored as source of possible changes in the deep-sea environment [179, 180]. A semi-rigid structure (the NESTOR *tower*), 360 m high and 32 m in diameter, equipped with 168 PMTs was designed to be used as "detection unit" for the neutrino telescope [181]. The basic element of the NESTOR tower is a hexagonal floor or star with two optical modules, one up-looking and the other down-looking, at the edge of each arm. The optical modules consists of a 15$''$ diameter photomultiplier tube enclosed in a spherical glass housing which can withstand the hydrostatic pressure up to 630 bar (fig. 34).

In March 2003 NESTOR deployed one tower floor, with a reduced size of 12 m and equipped with 12 PMTs, DAQ and transmission electronics, and associated environmen-

Fig. 34. – Concept of the NESTOR tower.

tal sensors. The electronics is placed at the center of the floor, housed in a 1 meter diameter titanium sphere. The cable for connection to shore, previously deployed at 3850 and connected to the off-shore station, was brought to the surface so that the floor was attached, cabled and redeployed to a depth of 3800 m [182]. This array was operational for about one month and the 745 down-going muon reconstructed events allowed to measure the cosmic-ray muon flux at the installation depth. As shown in fig. 35, good

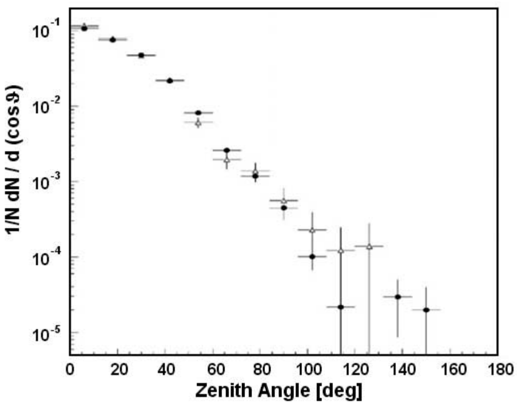

Fig. 35. – Distribution of the zenith angle of reconstructed tracks for the data (open triangles) and Monte Carlo (solid points) event samples [183].

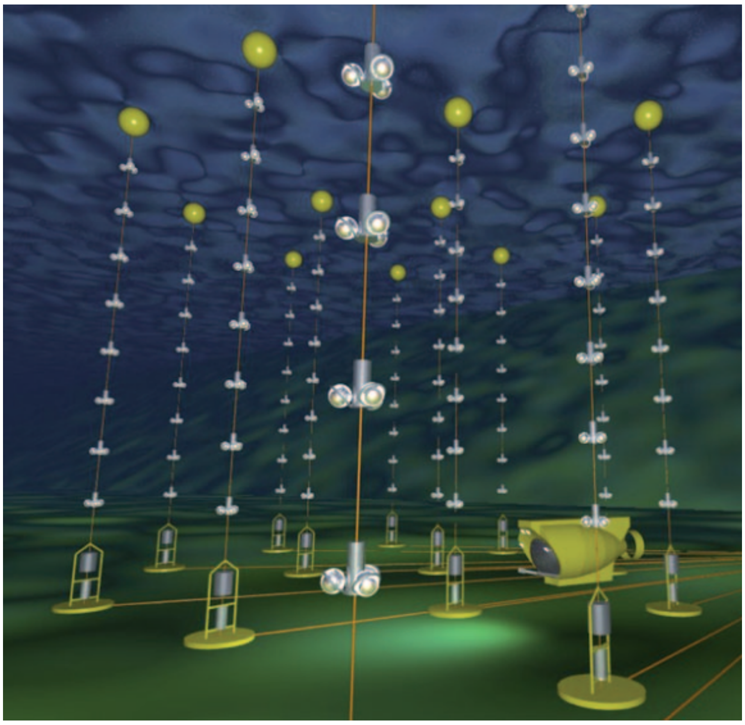

Fig. 36. – Pictorial view of the ANTARES detector.

agreement was found between distribution of the zenith angle of reconstructed tracks between data and Monte Carlo event samples [183].

8˙5. *ANTARES*. – Astronomy with a Neutrino Telescope and Abyss environmental RESearch (ANTARES) with nearly 900 optical modules, is at present the largest neutrino telescope operating in the Northern Hemisphere [185]. The R&D activities towards the construction of a deep-sea neutrino telescope demonstrator of limited size, started in 1996 including site evaluation campaigns and the construction of some prototype lines that allow to test critical components and technologies. ANTARES, see fig. 36 is made of 12 strings, 60 m apart, equipped with 25 storeys consisting of 3 pressure-resistent Optical Modules each one containing a 10″ down-looking PMT oriented at 45°. The spacing between storeys is 14.5 m. The covered footprint is about 0.1 km^2. The detector design was optimized for the detection of up-going tracks. The strings are moored at a depth of 2400 and interlinked in a Junction Box connected with a 45 km long electro-optical cable to the shore station at La Seyne sur Mer (close to Toulon, France). The site shows stable underwater currents, but a largely variable optical background due to a bioluminescence activity that can reach values of several hundreds kHz [186].

The data transmission is based on the "all data to shore" concept therefore all PMT signals above a 0.3 photo-electron threshold are sent to shore where a computer farm performs the filtering. Several different triggers looking for specific neutrino signals are implemented. Thanks to its high PMT granularity, the ANTARES telescope has an energy neutrino threshold of about 20 GeV for reconstructed muon events and detector

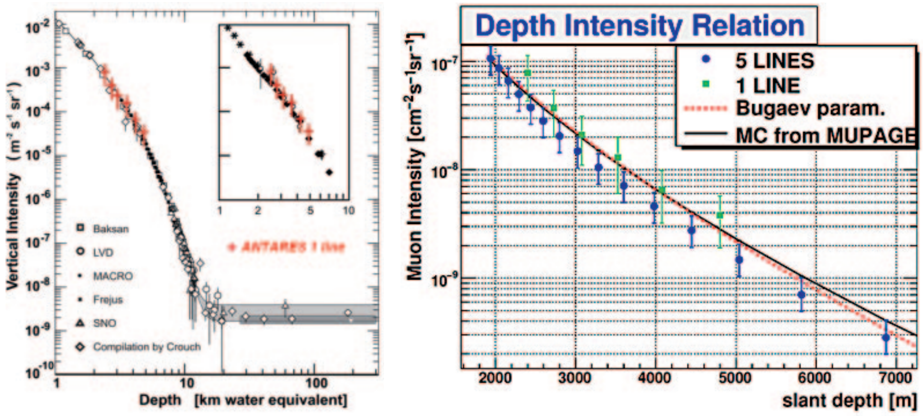

Fig. 37. – Depth *versus* muon flux intensity relation measured with ANTARES for 1 line (left) and 5 lines (right), respectively.

performance dramatically improves with increasing energy reaching at neutrino energy of 10 TeV an angular resolution of 0.3 degrees [184].

Data taking started in March 2006 after the deployment of the first detector line and by January 2007 five lines were deployed while the 12 line telescope was completed in May 2008 [185].

Data with one and five lines have been analysed and results have been presented, while data of the whole telescope are at present under analysis. The comparison of data events with simulated atmospheric neutrinos and muons exhibits a good agreement indicating that the response of the detector is well understood.

In particular the atmospheric muon flux as a function of slant water depth was measured, as shown in fig. 37, indicating good agreement between ANTARES data, other measurements and expectations. A detailed analysis of atmospheric muon events is reported in [187].

The search for cosmic neutrino point-like sources was performed using 140-days five-line data taking, with binned and unbinned analysis. A neutrino signal was searched from 25 possible source candidates including SNRs, microquasars, AGNs and the Galactic Center [188]. A different approach involved a blind search over the whole sky. Although no significant excess was found, the sensitivity obtained, shown in fig. 43, represents the best existing limits for point-like neutrino sources in the Southern Sky, even if compared to the multi-year experiments MACRO [189] and SuperKamiokande [190]. The predicted sensitivity of one-year lifetime for the whole 12 lines ANTARES detector, also shown in fig. 43, is expected to improve the present limit for the Northern Hemisphere neutrino detectors, by about one order of magnitude.

The successful experience of ANTARES represents an important achievement in the field of deep underwater high-energy neutrino telescopes.

8˙6. *NEMO*. – The NEutrino Mediterranean Observatory (NEMO) Collaboration aims at developing and validating key technologies for a cubic-kilometre-scale underwater neutrino telescope [191]. In particular, the project aims at developing technologies that fulfil the requirements of costs and operations even at depths larger than 3000 m for a km^3 underwater telescope.

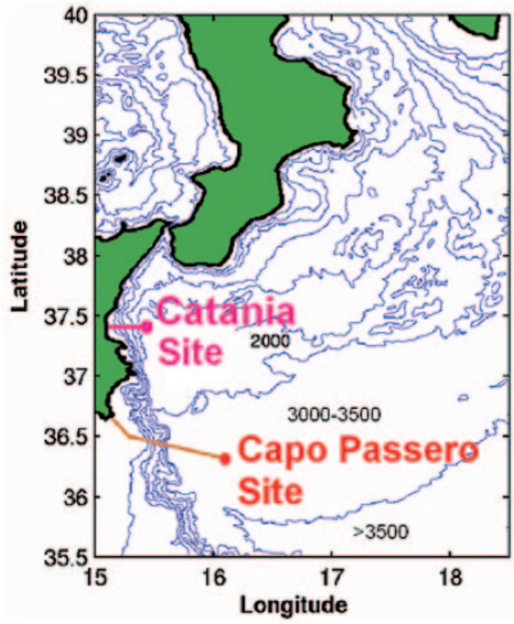

Fig. 38. – Geographic location of the Capo Passero site —latitude: 36° 30′ longitude: 016° 00′, depth 3500 m— and of the NEMO Test Site —latitude: 37° 30′, longitude: 015° 30′, depth 2100 m— offshore Catania, Sicily.

Moreover, more than 30 sea campaigns were performed by the NEMO Collaboration aiming at the search and characterization of a deep sea site for the installation of the km^3-scale detectors in the Mediterranean Sea. The NEMO Collaboration choose the Capo Passero site (fig. 38), located at a depth of 3500 m and 80 km off-shore the Sicily coast, that shows optimal features to host the km^3 detector: low optical background (30 kHz on 10″ PMTs at 0.5 s.p.e. threshold), blue light absorption length of 70 m (close to optically pure water), low currents (3 cm/s in average) and low sedimentation rate [192]. The site is located on a wide abyssal plateau, showing very stable environmental conditions and a flat seabed morphology over allowing for possible extension of the telescope.

The NEMO detector concept is based on semirigid vertical structures (the NEMO *towers*), see fig. 39, composed of a sequence of horizontal frames (named stories) made of marine grade aluminum. Each storey has two optical modules at either end, one looking vertically downwards and the other horizontally outwards and hosts instrumentation for positioning and environmental parameter monitoring. A tower, which consists of a sequence of stories interlinked by a system of ropes is anchored to the seabed and kept vertical by appropriate buoyancy on the top. The spacing between storeys is 40 m, while the distance between the anchor and the lowermost storey is 150 m. The structure is designed to be assembled and deployed in a compact configuration, and unfurled on the sea bottom under the pull provided by the buoy. Once unfurled each floor assumes an orthogonal orientation with respect to their vertical neighbors, obtaining a three-dimensional displacement of PMTs. Differently from the one-dimensional strings of PMTs, the tower allows disentangling of the muon azimuthal direction reconstruction even with data from only one structure.

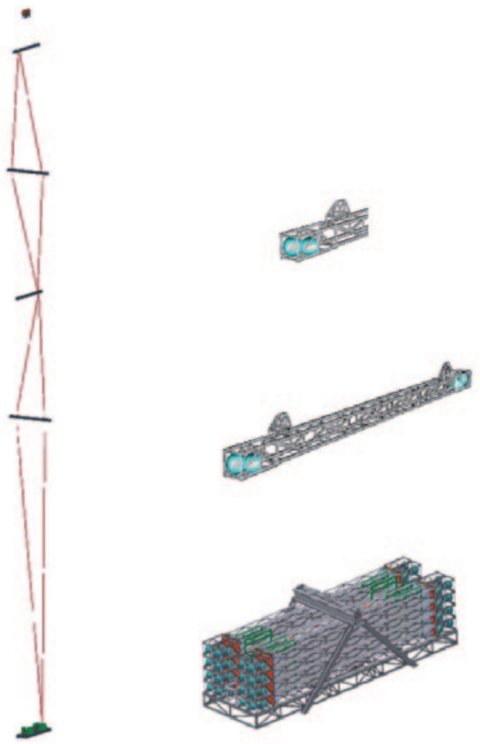

Fig. 39. – The NEMO *tower*. The length of each storey (*floor*) is 12 m and the inter-storey distance is 40 m. Thanks to the modular design of the tower, these parameters can be modified.

In order to validate the prototypes proposed for the km^3 detector, the Collaboration constructed a technological demonstrator at the NEMO Test Site, 2100 m undersea, located 25 km off-shore the Port of Catania (Sicily, Italy). The NEMO Phase-1 project started in 2002 and it was completed in December 2006 with the deployment and connection of a submarine Junction Box and a 4-floors prototype NEMO tower (called *mini-tower*) [193].

All the key components of an underwater neutrino detector were included: optical and environmental sensors, power supply, front-end electronics and data acquisition, time and PMT position calibration systems, slow control systems, on-shore data processing [194]. Five-month data were analyzed that gave information on the correct behavior of the apparatus, thus providing an important test for the tower design, construction and operation. Data allowed the measurement of the vertical muon intensity as a function of the angular distribution of the muon flux, see fig. 40. Though these data are collected with only one tower and a rather limited number of PMTs, very good agreement was found between data and simulation, confirming the optimal performances of the tower in muon reconstruction [195].

The project is now undergoing the NEMO Phase 2, that is the installation of an infrastructures for an underwater neutrino telescope, at the Capo Passero site. The NEMO Phase-2 infrastructure includes a shore laboratory located in the harbor area of Portopalo di Capo Passero, an 80 km long electro-optical cable which links a shore station

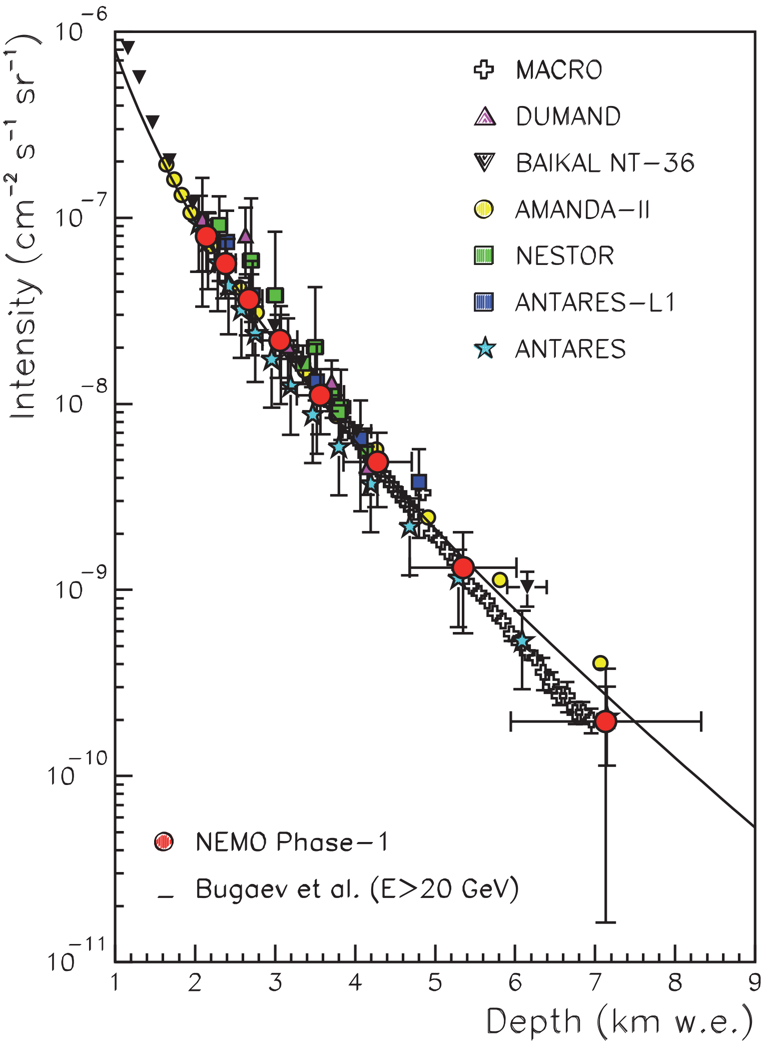

Fig. 40. – Atmospheric muon flux as a function of slant depth measured with the NEMO Phase-1 detector. Data from previous measurements and the parameterization of Bugaev are also reported for comparison.

to the underwater infrastructure, consisting of a main Junction Box (JB) used to connect detector prototypes and structures. The JB receives 10 kVDC from shore and distributes 400 VDC power supply to the underwater instrumentation. The total available power for Phase-2 project is 10 kW, to be soon implemented up to 60 kW. The experience gained with the NEMO Phase 1 led to a revision of the NEMO tower design aimed at simplifying the tower integration and reducing construction costs. In 2010, a prototypal *tower*, taken into consideration for the KM3NeT telescope as a complete prototype of detection unit, will be constructed and eventually deployed in the Capo Passero site. The *tower* will be equipped with 20 stories of 6 meters length, optical modules, environmental sensors, hydrophones, data acquisition and transmission electronics, power supply and distribution electronics, and a electro-optical cabling system [191].

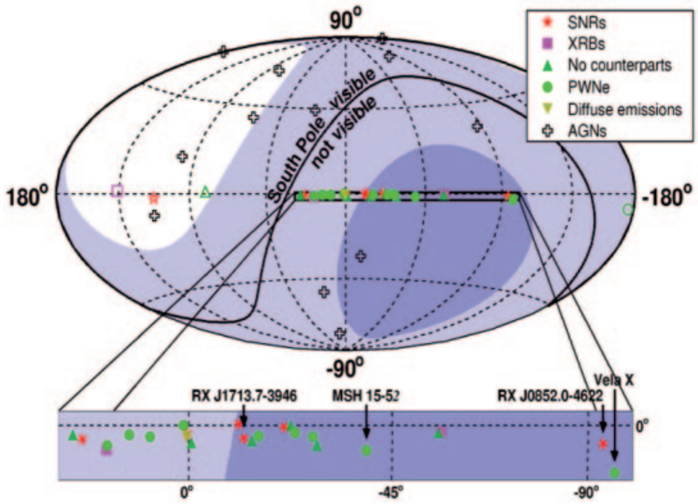

Fig. 41. – Sky visibility to up-going neutrinos for IceCube (solid line) and the one expected for KM3NeT (turquoise > 18 h per day, cyan > 6 hours per day). The position of a sample of identified TeV gamma sources is also shown. The insert represents a portion of the Galactic Plane.

8'7. *KM3NeT: towards a km*^{3}*-scale detector in the Mediterranean Sea.* – The KM3NeT consortium, funded by the EU aims at the construction of a cubic-kilometre-scale neutrino telescope in the the Northern Hemisphere with an integrated platform for earth and deep-sea sciences [196]. KM3NeT profits from the experience accumulated within the three pilot neutrino telescope projects operating in the Mediterranean Sea (ANTARES, NEMO, and NESTOR), whose members participate in the consortium together with members from other institutions, including ocean science laboratories. The telescope location in the Mediterranean Sea, due to the Earth rotation, will allow to see up-going neutrinos from about $3.5\,\pi$ and to survey of a large part of the Galactic Plane, including the Galactic Centre. In particular, the most intense SuperNova Remnants known to date, RXJ1713.7-3946 and Vela-Jr (RXJ0852.0-4622) that are both in the field of view of KM3NeT with a good visibility. Figure 41 shows the sky coverage of a neutrino telescope located in the Mediterranean Sea compared to the one of IceCube. A major advantage of a deep-sea cubic-kilometre-scale neutrino telescope is its angular resolution, around $0.1°$ above 30 TeV, indeed, a good point spread function allows to increase the signal-to-background ratio in neutrino point-like source searches thus improving the sensitivity. The goal of the project is to achieve a sensitivity for point-like sources of about $1 \cdot E_\nu^2 \Phi_\nu \simeq 10^{-9}\,\mathrm{GeV\,cm^{-2}\,s^{-1}}$ in 1 year [155].

In April 2008 the KM3NeT consortium reached an important milestone with the publication of the Conceptual Design Report (CDR) for the telescope. The Design Study phase (KM3NeT-DS) will culminate at the end of 2009 with the KM3NeT Technical Design Report (TDR) proposing technologies and the expected physics performance of the future detector. In parallel, since March 2008, a KM3NeT Preparatory Phase project (KM3NeT-PP, EU FP7) is addressing the political, funding, governance and strategic issues that need to be settled before the start of construction.

Three candidate sites, shown in fig. 42, were proposed by the ANTARES, NEMO and NESTOR Collaborations. The site choice as well as the possibility of a multi-site option

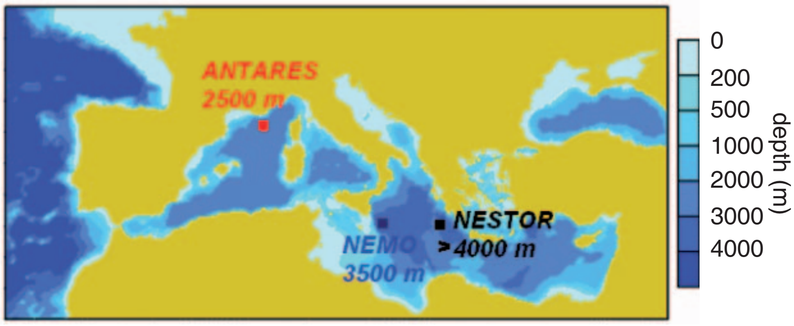

Fig. 42. – Geographic location of the three sites candidate for the installation of the Mediterranean km^3 detector.

is one of the strategic issues that will be addressed in KM3NeT-PP [197].

The investigation of the possible technical solutions concerning all the aspects of the design, construction, installation and maintenance of the telescope and their impact on physics performance is a major goal of KM3NeT. Several options for photo-sensors housed in pressure-resistant glass spheres have been studied: one or two large PMTs (8″ or 10″), or several 3″ PMTs per OM.

Following the concept of "all data to shore", all PMT signals above a given threshold (typically 1/3 of a single photo-electron) will be sent to the shore. The overall data rate will be of the order 100 Gb/s. On shore, a computer farm will perform the online filtering to reduce this rate by about 5 orders of magnitude.

Different options exist for the electronics performing the digitisation of the PMT signals and handling their transport to the shore. Due to the large path and data rates, optical fibers will be mandatory for the communication from the shore to the basis of the

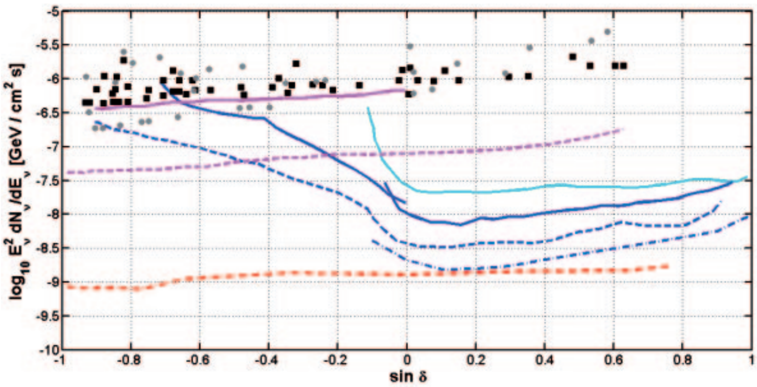

Fig. 43. – Sensitivity to E^{-2} neutrino point sources as a function of source declination for AMANDA (1387 days, cyan solid line), IC22 (276 days, blue dotted line: up-going ν, blue dash-dotted line: down-going ν), ANTARES 5 lines (magenta solid line), SuperKamiokande (black squares) and MACRO (light gray circles). The estimated sensitivity for IceCube (unbinned method: IC40 (1 year, blue dashed line), IC80 (1 year, blue solid line)) and the preliminary sensitivity for KM3NeT (1 year, binned method).

detection units, while the data transmission along the detection units themselves could be performed by copper wires as well as by optical fibers.

Concerning the mechanical structures, which is strongly linked to the deployment method, two major options are envisaged: detection units without horizontal extent (*strings*), and detection units with horizontally extended storeys (*towers*). The former solution can carry one multi-PMT OM per storey, or several OMs housing a single large PMT each. The latter solution, based on the principle developed by the NEMO Collaboration, is made of horizontal arms of a few meters length carrying 4 or 6 OMs each. For the deployment of NEMO-like towers, a compact configuration is deposited on the sea bed, and then an acoustic signal triggers the unfolding of the tower, under the buoyancy of a buoy at its top. The wet connections between towers and junction boxes are then performed with a Remotely Operated Vehicle. Monte Carlo simulations indicate that a telescope made of towers allows a better reconstruction of the induced muon tracks. In particular, a three-dimensional disposal of the the optical module allows to solve ambiguities in the azimuthal angle [198].

Full Monte Carlo simulation for the optimisation of the telescope has been performed [199-203] and the results will be presented in TDR [197]. The sensitivity to point-like sources with E^{-2} spectrum, for the KM3NeT detector is shown in fig. 43.

The KM3NeT infrastructure will also provide interfaces for earth and marine science instrumentation. It is foreseen that such devices are installed both in the neutrino telescope volume, if they are compatible and complementary, and in dedicated marine science nodes at some distance to the neutrino telescope to avoid adverse interferences.

9. – Ultra-High-Energy neutrino detection

The underwater optical Čerenkov technique is at present the most powerful tool for the investigation of astrophysical neutrino fluxes in the energy range between 1 TeV and 10 PeV. At higher energies, instead, the expected neutrino flux is so low that km^3-scale detectors are too small to detect UHE neutrino events. The distance between structures hosting optical sensor is, indeed, of the order of 100 m, due to light absorption length in water and ice. Therefore the cost of sensors, hardware, deployment and installation limits the affordable detector size to about some km^2 effective area for neutrino-induced muons, which is not enough for the detection of the expected neutrino fluxes at $E_\nu > 100\,\mathrm{PeV}$. For this reason different, complementary techniques have been investigated with the aim of observing extremely high-energy neutrino events, *e.g.* GZK neutrinos.

These techniques rely on the identification of a UHE neutrino interaction through the detection of coherent radiation — produced by neutrino-induced cascades — that propagates in dense media for very large distances. Hadronic showers, produced at the vertex of the UHE neutrino interaction, or electromagnetic showers, produced by e outgoing a ν_e interaction, radiate coherent radio and acoustic emissions. Radio waves have typical attenuation lengths of few km in the ice and the attenuation length for acoustic waves in the sea is also of the order of several km. Therefore, a sparse array of acoustic or radio sensors can be used to reconstruct the UHE ν interaction vertex.

9·1. *Askaryan radiation detection technique.* – Askaryan first suggested that natural media such as the polar ice-cap, salt domes and the lunar regolith could provide huge target material for neutrino interaction, being at the same time optimal transparent radiators for electromagnetic Radio Frequency (RF) signals [149]. In fact all of these approaches are now being explored. In such media, particle cascades induced by ultra-high-energy neutrinos are very compact, consisting of a bunch of relativistic charged particles displaced in a volume of a few dm^3, which develops at the speed of light over a distance of few tens meters from the vertex of the neutrino interaction, before dissipating its energy into residual ionization in the medium. The average number of electrons and positrons near total shower maximum is of order the cascade energy, E_c, expressed in GeV: $N^{e^+e^-} = E_c/10^9$. During the e.m. cascade development a negative charge accumulates due to Compton scattering of photons and to annihilation of positrons interacting with the medium's electrons. The charge asymmetry is about 20% at the shower maximum. The relativistic motion of this negative charge, distributed in a volume of few cm^3, in the medium produces coherent Čerenkov radiation in the RF range $f \simeq 100$ MHz–1 GHz.

A set of experiments at the Stanford Linear Accelerator center have now clearly confirmed the effect and described the radio signals shape, waveform, and amplitude *versus* deposited energy relation [204, 205]. In Antarctic ice, where the refraction index at these frequencies is $n \simeq 1.8$, the Čerenkov angle is is at about 56 degrees, with a few degree spread along the shower track. Different experiments are now pursuing the measurement of the GZK neutrino fluxes through the Askaryan radio technique.

9·1.1. Ice-based experiments. As described above, Askaryan radio pulses produced by UHE neutrino interaction in ice can be detected using an array of radio receivers buried in bulk ice [206].

The RICE (Radio Ice Čerenkov Experiment) experiment, located at the South Pole, consisted of a 20-channel array of dipole radio receivers, displaced on a 200 m ×200 m ×200 m cube, at 100–300 m depths above the AMANDA strings [207].

Beyond RF signal shape and amplitude, vertex reconstruction is the most direct discriminator of surface-generated *versus* non-surface events, neutrino candidates. Using the full data-set accumulated from 1999 to 2005, RICE evaluated an upper limit of $E^2\Phi(E) = 6 \cdot 10^{-7}\,\text{GeV}\,\text{cm}^{-2}\,\text{s}^{-1}\,\text{sr}^{-1}$ on the incident neutrino flux in the energy regime between 10^{17} eV and 10^{20} eV, shown as a magenta solid line fig. 46. The differential sensitivity, corresponding to the inverse of the energy-dependent exposure (*i.e.* the effective area for UHE neutrinos × lifetime) scaled by the Poisson upper-limit factor (2.3 for 90% CL), is also shown in the same figure as a dotted magenta line [208-210].

Following the RICE experience the AURA (Askaryan Under-ice Radio Array) detector was deployed in shallow and deep ice. In particular, two AURA clusters were deployed on top of IceCube strings at depths of 1450 m and 250 m. AURA results are under analysis [211].

Another possibility is to detect the neutrino-induced radio pulses emerging from the polar ice-cap. ANITA (Antarctic Impulsive Transient Antenna) [212] is a Long Duration Balloon (LDB) experiment that flew above the South Pole in three different flights: the pilot experiment ANITA-lite, ANITA-1, and ANITA-2.

ANITA-1, shown in fig. 44, was an array of 32 dual-linear-polarization, quad-ridged horns, antennas arranged in upper and lower rings, each with 16 antennas [213]. The antennas working bandwidth is 200 MHz–1.2 GHz. The antennas were arranged in two rings, each with 16 antennas, pointing at 10° below the horizontal, to maximize sensitivity to the largest portion of the volume near the horizon. The combined view of all antennas covers the entire lower hemisphere down to nadir angles of about 55°, comprising 99.4% of the area within the horizon. ANITA was launched from Williams Field, Antarctica near McMurdo station, on December 2006, and accumulated a net exposure lifetime of 17.3 days with a mean ice depth in the field of view of 1.2 km. From balloon flight

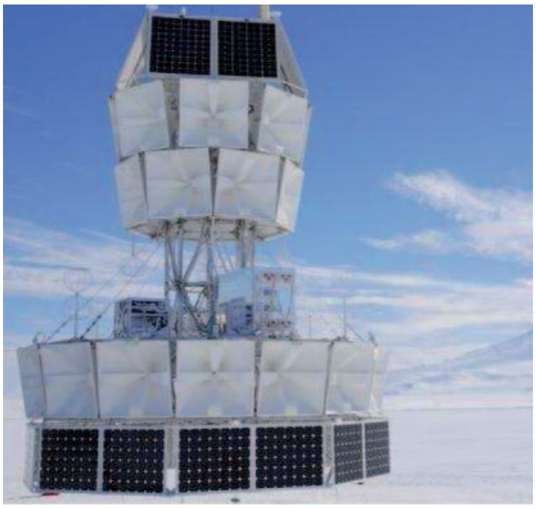

Fig. 44. – The ANITA-1 payload in launch configuration. Photovoltaic panels at the top and bottom, and antenna clusters are visible. The side of each square antenna mouth is about 0.9 m. The payload is about 8 m height.

altitudes of about 36 km above the sea level (corresponding to about 34 km above the ice-cap), the horizon is at nearly 700 km distance, giving a synoptic view of $\simeq 1.6\,\mathrm{Mkm}^2$ of ice, corresponding to about $2\,\mathrm{Mkm}^3$ volume of ice, taking into account $L_a^{RF} \simeq 1.2\,\mathrm{km}$. This large acceptance, while tempered by the limited exposure in time, still yields the largest sensitivity of any experiment to date for GZK neutrinos.

Among the total number of zero level triggering events, about $2 \cdot 10^6$, off-line analysis was carried on to select events showing the expected polarization, spectral and phase coherence, and vertexes far at least 50 km from sites polluted by anthropogenic electromagnetic interference (*e.g.* camps and paths). After these cuts a subset of 6 events was found. These events show an e.m. signal horizontally polarized, in contrast with the vertical polarized radio signal expected from Askaryan radiation refracted from ice to the atmosphere, thus they are not considered as neutrino events. Results of ANITA-1 [214] are shown in fig. 46, the dashed red line represents the differential sensitivity for neutrino fluxes; the integral sensitivity (fig. 46, red solid line) calculated on a pure E^{-2} spectrum for the energy range $10^{18.5}\,\mathrm{eV}$–$10^{23.5}\,\mathrm{eV}$ was evaluated to be $E_\nu^2 \Phi_\nu = 2 \cdot 10^{-7}\,\mathrm{GeV\,cm^{-2}\,s^{-1}\,sr^{-1}}$. On the other hand, the recorded 6 events seem to be fully consistent with geo-synchrotron emissions from an Extensive Air Showers (EAS) produced by an UHECR. A second launch of ANITA (ANITA-2) was carried out on December 2008 and had a successful 30 day flight over Antarctica, recording $27 \cdot 10^6$ events. Taking into account technological improvements and enhanced lifetime ANITA-2 is about a factor of 3 to 8 improvement over ANITA-1.

The experience acquired with ANITA, RICE and AURA merged into the IceRay project aiming at the realization of a $1000\,\mathrm{km}^2$ Ultra-High-Energy neutrino detector at the South Pole.

Another aim of IceRay is to look for coincident *hybrid*, events with the IceCube detector [215]. An UHE neutrino interaction can produce, in fact, both a shower at the ν interaction vertex and a long-ranged charged lepton with the potential for detection in both radio and optical channels. Hybrid event rates, for various GZK flux models, varies from few to about ten in a ten-year live-time. Despite such events are very rare, they are background-free, and would allow cross-calibration of the energy scale between IceCube and IceRay. Moreover the detection of these events in coincidence with the IceCube neutrino detector, will allow complete calorimetry, as described in subsect. **9**˙3 [216]. IceRay, as a first stage, aims at building a 50 km^2 array with the maximum sensitivity in the energy region of the GZK neutrino flux, around 10^{18} eV. Each station consists of three holes separated by 5–10 m, with four antennas (two of each polarization, horizontal and vertical) in each hole. Event directionality can be obtained even from a single-station. A test-bed IceRay station, consisting of 4 antennas, was deployed in austral summer 2009. The test-bed will provide year-round monitoring of the radio environment at the South Pole and it will facilitate further development of the 50 km^2 array.

9˙2. *Moon radio Čerenkov observations*. – As suggested by Dagkesamanskii and Zheleznykh, observations of the Moon with ground-based radio-telescopes can be used to search for cascades produced by UHE neutrino interactions. At UHE the neutrino-nucleon cross-section is such that neutrinos traversing the lunar diameter are severely attenuated. This causes the appearance of GHz Čerenkov signals originated almost entirely from the limb of the Moon [217].

The first attempt to use the lunar regolith in the search for UHE neutrinos was made at the 64 m Parkes radio telescope, Australia [218]. The Moon was observed for approximately 10.5 hours using a wide-bandwidth dual-polarisation receiver. No real events were identified. Subsequently the Goldstone Lunar Ultra-High-Energy Neutrino Experiment (GLUE) [219], ran at NASA Goldstone Deep-Space Communications Complex, USA, and RAMHAND [220], ran at the Kalyazin Radio Astronomical Observatory, Russia, also recorded null results. These results set the first constraints on UHE neutrino flux models such as Z-Bursts and Topological Defects.

The future plan for lunar Cherenkov observations foresee the utilisation of the planned SKA (Square Kilometre Array) radio array. In order to improve real-time discrimination of Cherenkov pulses from background noise and terrestrial radio-frequency interference, the full capabilities offered of such instruments in nano-second pulse detection will have to be exploited. This will require the latest in signal processing technology. In parallel, sophisticated simulations should be used to optimise observation parameters such as frequency, beam pointing position, and bandwidth [221].

9˙3. *The thermo-acoustic technique*. – Another technique for EHE ν detection is based on the identification of the acoustic signature of neutrino-induced showers in water. Though the studies on this technique are still in an early stage, its potential use to build very large neutrino detectors water is appealing, thanks to the optimal properties of water as sound propagator [222].

The idea of acoustic neutrino detection, first proposed by Askaryan in 1957 [223], is based on the reconstruction of hadronic and electromagnetic showers produced by neutrino interaction in dense media. As discussed above, both in the case of CC or NC interaction, the hadronic cascade carries about 25% of the neutrino's energy. In case of CC interaction of a ν_e, an e.m. shower is also produced close to the neutrino interaction vertex. The deposit of the cascade energy in a small volume of water, cylindrical in shape with a length L_c of few tens of metres and a few centimetres in radius r_c turns out in heating of the medium, therefore in its expansion(5). The typical time of the energy deposition along the shower axis, almost co-linear with the neutrino direction, is of the order of $L_C/c \simeq 10^{-7}$ s, while the expansion time is of the order of $r_c/c_{sound} \simeq 10^{-4}$ s. The net result is the coherent production of a mechanical wave, "pancake-shaped" propagating, in a homogeneous medium, perpendicularly to the shower axis.

Acoustic pulses from particle showers were first observed at Brookaven NL in 1979 [226], using a beam of 200 MeV protons with a total energy deposit in water of about 10^{18} eV. The pulse amplitude as a function of total energy deposition, water temperature and pressure was studied. The acoustic pulse production was recently confirmed by several experiments, using proton beams (in Uppsala and ITEP Moscow) and high-intensity laser beams (in Erlangen).

According to Learned's theoretical work [227], the acoustic pulse is bipolar, following the second time derivative of the temperature of the excited medium. The frequency spectrum of the signal is a function of the transverse spread ($r_{cascade}$) of the shower, with typical maximum amplitude in the range of few tens kHz. The amplitude of the bipolar signal is proportional to the deposited energy and to the medium properties: the thermal expansion coefficient (β), the sound velocity (c_s) and the specific-heat capacity (C_p). A rule of thumb to calculate the acoustic pulse amplitude at 1 metre produced by a neutrino of energy E_ν, impinging in a dense medium is

$$P_0 \simeq 0.25\ E_\nu \cdot \Gamma\ E_\nu/V_c \simeq 2\ \Gamma\ E_\nu \cdot 10^{-19}\ [\mathrm{Pa/eV}], \tag{9}$$

where V_c is the volume of the medium where the shower deposits its energy, the factor 0.25 is the fraction of E_ν (in units of [eV]) transferred to the shower and $\Gamma = c_s^2\beta/C_p$ is the (dimensionless) Gruneisen coefficient of the medium [228]. The Γ-coefficient for deep Mediterranean-Sea water is about 0.12, about a factor ten larger in polar ice and about 3.2 in compact mineral salt. Since, at frequencies of few tens kHz, acoustic pulses can travel large distances in ice, seawater and salt, these natural media can be used to build large volume neutrino detectors instrumented with sparsely spaced arrays of acoustic sensors.

Assuming radial propagation of the sound wave and that the sound absorption length in water is $L_a^{sound} \simeq 10$ km at 20 kHz, the pulse amplitude produced by a $E_\nu = 10^{20}$ eV neutrino, recorded at 1 km distance, is expected to be about 15 mPa. Ice, despite the Gruneisen coefficient is larger, suffer for a stronger sound absorption ($L_a^{sound} \simeq 300$ m, at about 400 m depth) compared to water.

The energy threshold for neutrino acoustic detection is set by the ratio between ambient noise and signal.

In the frequency range of interest for neutrino detection (10–40 kHz), the acoustic ambient noise amplitude in deep sea adds up about few mPa. This permits, in a first approximation, the discrimination of acoustic signals originated by neutrinos having $E_\nu > 10^{19}$ eV (assuming 1 km distance). The possibility to use time and direction coincidence can help to reduce the ambient noise by at least one order of magnitude. The absolute value of noise in deep ice has not been yet measured. Present data indicate a decrease

(5) This scenario is valid at energies below the LPM (Landau, Pomeranchuk, Migdal) effect energy regime [224, 225], $E \geq 10^{19}$ eV, that causes a strong reduction of the Bremsstrahlung and pair production cross-sections for e and γ, respectively and, therefore, a lower energy deposit per unit of volume.

of noise amplitude as a function of depth and a Gaussian distribution of amplitudes in deep ice [229].

In both media, moreover, sound refraction must be taken into account. Sound refraction is originated by change of sound velocity in the medium as a function of depth, due to different pressure and temperature (in ice and water) and salinity (in sea water). The effect of refraction is that the expected pancake-shaped neutrino-induced wave front becomes a hyperboloid in the real case.

Based on the previous considerations several groups have carried out simulations on future extremely large acoustic neutrino detectors. It is worth to mention, however, that acoustic detectors can be hardly used as "telescopes", due to the poor angular accuracy of the wave front reconstruction ($\simeq 10^{\circ}$).

Calculation performed by the ANTARES [230] and by the AMADEUS [231] groups indicate that a $1500\,\mathrm{km}^3$-detector deployed in deep seawater, made of about 200 sensors per km^3 may reach sensitivity at level of the WB limit for $E_\nu = 10^{20}\,\mathrm{eV}$ in few years. A different result was recently presented by the ACORNE group, that simulated the response of a dense array of 1100 acoustic modules displaced in a $1\,\mathrm{km}^3$ volume of seawater, anchored to the structures of a km^3 Čerenkov neutrino telescope. Sophisticated acoustic signal identification, based on matched filters, and reconstruction strategy of the acoustic wavefront geometry should allow to reach a sensitivity close to the Waxman-Bahcall limit for UHE neutrinos [232] in 10 years of data taking.

Another intriguing possibility is also to use a very large volume array of acoustic sensors both as independent detector and as a calorimeter for the (few, but almost background free) UHE neutrino events detected by the km^3 telescope. At energies greater than 10 PeV, the majority of neutrino-induced muon tracks, reconstructed by the km^3 optical telescope, are quasi-horizontal. For these events, the $\nu_\mu N \to \mu X$ interaction vertex is located several km outside the telescope. Clusters of acoustic modules, displaced in a large volume around the km^3 telescope, could be able to identify the acoustic signature generated by the hadronic cascade at the ν vertex. Once the ν vertex is located, thus the muon range is reconstructed, the total energy of the muon crossing the km^3 detector can be reconstructed. Despite the fact that, for independent acoustic detection, the neutrino energy threshold is high ($E_\nu > 10^{18}\,\mathrm{eV}$), the time and arrival direction correlation between optical and acoustic signals would help to strongly lower the acoustic detection energy threshold(6).

Thanks to the possibility to use also the optical, radio and acoustic techniques in ice, the SPATS (South Pole Acoustic Test Setup) group —aiming at R&D and tests for the construction of a large acoustic detector at the South Pole— has simulated a hybrid detector made of 80 IceCube strings plus an external ring of 13 strings deployed in holes at 1 km distance from the centre (2.5 km deep) and 91 radio/acoustic strings with a spacing of 1 km, 1.5 km deep. Monte Carlo simulations predict that, for optimistic GZK neutrino flux models, 16 events per year could be seen by the acoustic detector, and 8 in coincidence with the radio detectors: that would offer the potential for cross-calibration of signals from the different technologies [233].

On the experimental side, in recent, years the possibility of using hydrophones installed on military array and the infrastructures of new underwater/ice Čerenkov tele-

(6) An improvement of about one order of magnitude is expected using the information of the sound wave arrival direction, provided by the optical detector, to reduce the acoustic signal-to-background ratio.

Fig. 45. – Left: an acoustic module of AMADEUS, equipped with 6 hydrophones. Right: OνDE before the deployment.

scopes, has permitted to several experimental groups to start R&D activities on acoustic detection.

The SPATS team installed three acoustic test lines, each equipped with 7 transmitters and 7 receivers, within the IceCube detector. SPATS permitted the first studies of deep-ice acoustic properties, using calibrated pingers deployed at several depths and distances. The operation of SPATS permitted for the first time the experimental measurement of sound attenuation length and velocity in deep polar ice. Present results show that sound attenuation length in ice is about 300 m, a value much less than expected from theoretical estimates [234].

The SAUND (Study of Acoustic Ultra-high energy Neutrino Detection) collaboration uses the AUTEC naval array of wide band hydrophones deployed at $\simeq 1500$ m depth offshore Bahamas. SAUND recorded 15 days of data reading out 6 hydrophones at the site, displaced in a $\simeq 7\,\mathrm{km}^2$ wide area and obtained the first limit of the UHE neutrino using the acoustic technique [235, 236]. In the second phase of SAUND, data from 56 hydrophones, covering an area of about $1000\,\mathrm{km}^2$ were recorded for 120 days, aiming at reaching 1 year of data acquisition. SAUND phase 2 is currently active and is also permitting a detailed characterisation of deep sea noise as a function of frequency and direction [237].

In the framework of the activities of the ANTARES neutrino telescope, the AMADEUS (ANTARES Modules for Acoustic Detection Under the Sea) group has deployed few tens of hydrophones onboard two strings. Hydrophones are both commercial piezo-ceramic hydrophones (see fig. 45), self-made piezo-ceramic hydrophones and self-made hydrophones hosted in and acoustically coupled with $17''$ pressure-resistant glass spheres that currently house the ANTARES PMTs. The system permitted the monitoring of deep-sea noise in the site and sound source tracking. AMADEUS could easily identify and locate signal emitted by the beacon used for the ANTARES acoustic positioning system and from biological sources [238].

The NEMO Collaboration is also conducting the first studies for acoustic neutrino detection. In 2005 the Collaboration deployed OνDE (Ocean Noise Detection Experiment) at the NEMO Test Site, 2000 m depth, 25 km off the coast of Sicily. OνDE, that was successfully recovered on April 2008, comprises four hydrophones arranged on a pyramidal-shaped (see fig. 45) mounting and low-cost electronics for data acquisition and transmission. Data (sampled at 96 kHz and with 24 bit resolution) were transmitted in real-time from deep sea and recorder on shore. Acoustic noise was studied as a function of time, weather conditions, presence of ships and biological sources, with important drawbacks in bio-acoustics [239]. Based on the experience of OνDE, the NEMO Collaboration is designing an innovative acoustic position system for the km^3 detector that will be installed on the KM3NeT *tower* prototype to be deployed in Capo Passero. The system, an array about 30 hydrophones, will be able to work both as positioning system and acoustic detector, in coincidence with the optical detector [240].

9˙4. *Neutrino extensive air shower detection.* – Another method for looking at UHE neutrinos is the reconstruction of quasi-horizontal extensive atmospheric showers, initiated by CC or NC neutrino interaction in very deep atmosphere (close to ground) or looking at up-going showers in atmosphere initiated by the decay products of an emerging (Earth-skimming) τ lepton, after the propagation and interaction of a UHE ν_τ inside the Earth [152].

Analysing atmospheric showers reconstructed by the surface array detector of Auger, a search for UHE neutrinos in the energy range 10^{17} eV–10^{19} eV, could be afforded.

Identification of neutrino-induced showers in the much larger background of the ones initiated by nucleonic cosmic-rays is based on the idea that neutrinos can penetrate large amounts of matter and generate "young" inclined showers developing close to the ground. In contrast UHE nuclei interact within a few tens of $\mathrm{g \cdot cm^{-2}}$ after entering the atmosphere, producing "old" showers with shower fronts narrower in time. The Fast ADC installed on the surface detector tanks, allows to distinguish the narrow signals in time, expected from a shower initiated high in the atmosphere, from the broad signals expected from a young shower [241].

On the other hand, air fluorescence detectors, such as HIRES [243, 242] and Auger-FD (Fluorescence Detector), and the Auger-SD (Surface Detector) were used to observe upgoing showers produced by the decay of τ. Tau may originate in the interaction of an upgoing or Earth-skimming ν_τ close to the Earth surface or inside a mountain.

Contrary to other flavours, in fact, the interaction of a UHE ν_τ inside the Earth generate a τ lepton that decays again in a ν_τ. This is equivalent to an energy loss process that ends when the ν_τ has an energy such that the neutrino absorption length in the Earth is larger than the residual distance between the newly generated ν_τ and the Earth ground. Assuming a $\Phi_\nu(E) = k \cdot E_\nu^{-2}$ flux Auger obtained a 90% C.L. limit on the all-flavour neutrino flux (using down-going showers) of $k < 3.2 \cdot 10^{-7}\,\mathrm{GeV\,cm^{-2}\,s^{-1}\,sr^{-1}}$ shown in fig. 46. In the same figure is shown the limit for Earth-skimming up-going neutrinos $k < 4.7 \div 2.5 + 2.2 \cdot 10^{-8}\,\mathrm{GeV\,cm^{-2}\,s^{-1}\,sr^{-1}}$, where the upper/lower values correspond to best/worse scenario of systematics. The limit in differential format, proportional to the inverse of the detector exposure as a function of energy, is also shown to highlight the energy range at which the detector is more sensitive [244].

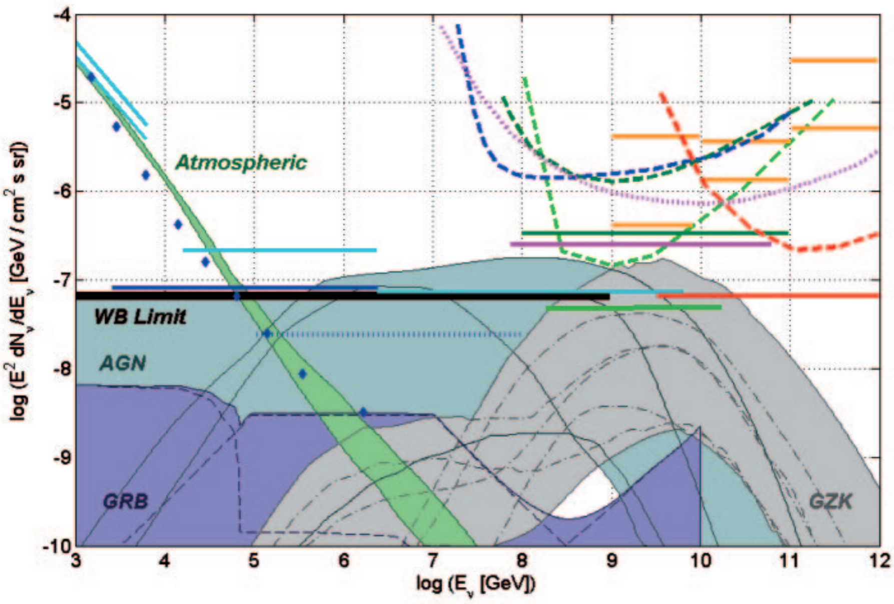

Fig. 46. – Expected HE neutrino fluxes and present limits measured by different experiments. Theoretical atmospheric neutrino flux (light green area): upper line horizontal ν, lower line vertical ν. Waxman Bahcall bound (black solid line). Expected cumulative AGN neutrino fluxes: the blueish area corresponds to maximal-flux models. Expected GRB neutrino flux for $\Gamma = 300$ and $z = 2$: the violet area is the sum of different contribution reported in dashed lines; precursor ($E < 10^5$ GeV), prompt (10^5 GeV $< E < 10^{8.5}$ GeV), afterglow ($E > 10^{8.5}$ GeV). Expected GZK neutrino flux: the greyish area corresponds to maximal-flux models. Experimental data from AMANDA-II (solid cyan line): measured ν_μ flux ($E < 10^4$ GeV), sensitivity to upgoing astrophysical ν_μ (10^4 GeV $< E < 10^{6.5}$ GeV), sensitivity to ν-induced cascades ($10^{6.5}$ GeV $< E < 10^{10}$ GeV). Experimental data from IceCube: IC22 measured ν_μ flux (blue diamonds), sensitivity to upgoing astrophysical ν_μ (solid blue line), sensitivity to ν-induced cascades (dashed blue line), expected IC80 sensitivity to astrophysical ν_μ (dotted blue line). Experimental data from RICE: sensitivity to ν-induced cascades (magenta solid line), differential sensitivity to ν-induced cascades (magenta dotted line). Experimental data from ANITA: sensitivity to ν-induced cascades (red solid line), differential sensitivity to ν-induced cascades (red dotted line). Experimental data from Auger: sensitivity to upgoing ν_τ (light green solid line) and downgoing ν (dark green solid line), differential sensitivity to ν_τ-induced cascades (light green dashed line) and downgoing ν (dark green dashed line). Experimental data from HIRES: sensitivity to ν_τ (yellow solid line) and ν_e (orange solid line).

10. – Conclusions

High-energy neutrino telescopes are "discovery" instruments that are expected to gather unique pieces of information for the comprehension of the High-Energy Universe. These detectors have high potential to solve several crucial questions in astroparticle physics such as the origin of Cosmic Rays, the investigation of hadronic processes in extreme astrophysical environments and the identification of UHECR sources.

An important contribution to the design and optimization of both HE and UHE neutrino telescope comes from the results obtained by VHE gamma and UHECR experiments.

In particular VHE gamma astronomy has reached in last few years a maturity level that allows, at least for some specific classes of Galactic sources, to obtain reasonable estimates of expected HE neutrino fluxes. Concerning the UHECR results, the discrepancy between HIRES and Auger experiments about the mass composition, introduces a very large uncertainty on the estimate of GZK (BZ) neutrino fluxes.

Perspectives for HE neutrino detection have dramatically improved in the last decade due to the huge technological progresses. At South Pole, IceCube, with 59 strings deployed over 80 and the completion expected by 2011, is about to reach the sensitivity region below the Waxman and Bahcall limit where, in the hypothesis of extragalactic proton dominance at $E > 10^{19}$ eV, neutrino signals from cosmic sources are expected to be detected.

On the other hand, after many years of activities focused to prototyping and validation of deep-sea technologies, mainly undertaken by the collaborations operating in the Mediterranean Sea, the KM3NeT consortium is ready for the start-up of the construction phase of the km^3 scale underwater neutrino telescope in the Mediterranean.

KM3NeT will cover a large fraction (about $3.5\,\pi$) of the sky, for up-going neutrinos, where RXJ1713.7-3946 and Vela Jr. are visible for more than 18 hours per day.

Great progresses have also been made towards the detection of UHE neutrinos: the sensitivity reached by ANITA and Auger allows to exclude the exotic *top-down* models.

Moreover, after the results of several pioneering experiments, a very large array based on radio Čerenkov techniques, IceRay, is proposed at the South Pole. On the other hand, an intense R&D activity is undergoing for example in the field of acoustic detection, that although has not yet reached the maturity level of the radio Čerenkov technique, is a promising approach that can be exploitable for the UHE neutrino detection underwater.

We believe that the observation of the Universe in the "neutrino light" will play a major role in the multi-messenger astronomy providing a new insight on the far and violent Universe.

* * *

The authors are deeply grateful to E. Migneco, C. Distefano, R. Coniglione and F. Vissani for helpful discussions, suggestions and reviews. We also thank the anonymous referee who helped us to improve the manuscript with his/her precious comments.

REFERENCES

[1] Lipari P., *Proc. Neutrino Oscillation (Venice, Italy)*, (2008) arXiv:0808.0417.
[2] Greisen K. *et al.*, *Phys. Rev. Lett.*, **16** (1966) 748.
[3] Zatsepin G. T. and Kuzmin V. A., *JETP Lett.*, **4** (1966) 78.
[4] Mangano G. *et al.*, *Nucl. Phys. B*, **729** (2005) 221.
[5] Bahcall J. N. and Pinsonneault M., *Rev. Mod. Phys.*, **64** (1992) 64.
[6] Ahmad Q. R. *et al.*, *Phys. Rev. Lett.*, **87** (2001) 071301.
[7] Davis R. *et al.*, *Phys. Rev. Lett.*, **20** (1968) 1205.
[8] The SuperKamiokande Collaboration, *Phys. Rev. Lett.*, **82** (1992) 2644.
[9] Hirata K. *et al.*, *Phys. Rev. Lett.*, **58** (1987) 1490; Hirata K. *et al.*, *Phys. Rev. D*, **38** (1988) 448.
[10] Bionta R. M. *et al.*, *Phys. Rev. Lett.*, **58** (1987) 1494; Bratton R. B. *et al.*, *Phys. Rev. D*, **37** (1988) 3361.
[11] Alekseev E. N. *et al.*, *JETP Lett.*, **45** (1987) 589; Alekseev E. N. *et al.*, *Phys. Lett. B*, **205** (1988) 209.
[12] Berezinsky V. S. and Zatsepin G. T., *Phys. Lett. B*, **28** (1969) 423.

[13] Hess V., *Phys. Z.*, **13** (1913) 1084.
[14] Pacini C., *Nuovo Cimento*, **6** (1912) 93.
[15] Gaisser T. K., *Cosmic Rays and Particle Physics* (Cambrige University Press, Cambrige) 1990.
[16] Cronin J. W., Gaisser T. K. and Swordy S. P., *Sci. Am.*, **276** (1997) 44.
[17] Fermi E., *Phys. Rev.*, **75** (1949) 1169.
[18] Bell A. R., *Mon. Not. R. Astron. Soc.*, **182** (1978) 147.
[19] Hillas A. M., *Annu. Rev. Astron. Astrophys.*, **22** (1984) 425.
[20] Ginzburg V. L. and Syrovatsky S. I., *Origin of Cosmic Rays* (Pergamon, New York) 1964.
[21] Berezinsky V., *J. Phys. Conf. Ser.*, **120** (2008) 012001.
[22] Butt Y., *Nature*, **460** (2009) 7256.
[23] Abdo A. A. *et al.*, *Phys. Rev. Lett.*, **101** (2008) 221101.
[24] Anemori M. *et al.*, *Science*, **314** (2006) 439.
[25] Vernetto S. *et al.*, *Proc. 31st ICRC, Lodz, Poland* (2009).
[26] Abbasi R. *et al.*, *Proc. 31st ICRC, Lodz, Poland* (2009).
[27] Abdo A. A. *et al.*, *Astoph. J.*, **688** (2008) 1078.
[28] Takeda M. *et al.*, *Phys. Rev. Lett.*, **81** (1998) 1163.
[29] Abbasi R. *et al.*, *Astropart. Phys.*, **32** (2009) 53.
[30] Abbasi R. *et al.*, submitted to *Phys. Rev. Lett.*, arXiv:0910.4184.
[31] Abbasi R. *et al.*, *Proc. 31th ICRC, Lodz, Poland* (2009), arXiv:0906.2319.
[32] Waxmann E. and Bahcall J., *Phis. Rev. Lett.*, **78** (1997) 2292.
[33] Biermann P. and Strittmatter P. A., *Astrophys. J.*, **322** (1997) 643.
[34] The Pierre Auger Collaboration, *Science*, **318** (2007) 938.
[35] Véron-Cetty M. P. and Véron P., *Astron. Asrtophys.*, **455** (2006) 773.
[36] Hague J. D. for the Pierre Auger Collaboration, *Proc. 31st ICRC, Lodz, Poland* (2009).
[37] Tueller J. *et al.*, *Astrophys. J.*, **681-1** (2008) 113.
[38] Gorbunov D. *et al.*, *JETP Lett.*, **87** (2008) 461.
[39] The Hires Collaboration, *Phys. Rev. Lett.*, **100** (2008) 101101.
[40] Abraham J. for the Pierre Auger Collaboration, *Phys. Rev. Lett.*, **101** (2008) 06110.
[41] Soomers P. for the Pierre Auger Collaboration, *Proc. 31st ICRC, Lodz, Poland* (2009).
[42] Wahlberg H. for the Pierre Auger Collaboration, *Proc. 31st ICRC, Lodz, Poland* (2009).
[43] Aloisio R., Berezinsky V. and Gazizov A., arXiv:0907.5194v1 (2009).
[44] Tanimori T. *et al.*, *Astrophys. J. Lett.*, **429** (1994) L61.
[45] de la Calle Pérez I. *et al.*, *Astrophys. J.*, **599-2** (2003) 909.
[46] Aharonian F. *et al.*, *Astrophys. J.*, **539** (2000) 317.
[47] Albert J. *et al.*, *Astropart. Phys.*, **23** (2005) 493.
[48] Aharonian F. *et al.*, *Nature*, **432** (2000) 75.
[49] Acciari V. A. *et al.*, *Astrophys. J. Lett.*, **684** (2008) L73.
[50] Aharonian F., *Science*, **315-5808** (2007) 70.
[51] De Angelis A. *et al.*, *Riv. Nuovo Cimento*, **31** (2008) 131.
[52] Costamante L. and Ghisellini G., *Astron. Asrtophys.*, **56** (2002) 384.
[53] Spandre G. *et al.*, *Nucl. Instrum. Methods A*, **572** (2007) 500.
[54] Tibolla O. for the HESS Collaboration, *Proc. 31st ICRC, Lodz, Poland* (2009), arXiv:0907.0574v1.
[55] de Jager O. C. *et al.*, arXiv:0906.2644.
[56] Aharonian F. *et al.*, *Rep. Prog. Phys.*, **71** (2008) 096901.
[57] Bartko H. *et al.*, *Proc. 23th ICRC, Pune, India* (2005).
[58] Aharonian F. *et al.*, *Astron. Asrtophys.*, **477-1** (2008) 353.
[59] Gonzales-Garcia M. C., Halzen F. and Mohapatra S., *Astropart. Phys.*, **31-6** (2009) 437.

[60] de Jager O. C. *et al.*, *Astrophys. J.*, **689** (2008) L125.
[61] Funk J., *Proc. 30th ICRC, Merida, Mexico* (2007).
[62] Abdo A. A. *et al.*, *Astrophys. J.*, **695** (2009) L72.
[63] Tanaka T. *et al.*, *Astrophys. J.*, **685-2** (2008) 988.
[64] Aharonian F. *et al.*, *Astron. Asrtophys.*, **464-1** (2007) 235.
[65] Helder E. A. *et al.*, *Science*, **325-5941** (2009) 719.
[66] Aharonian F. *et al.*, *Astron. Asrtophys.*, **437-1** (2005) L7.
[67] Gabici S., Aharonian F. and Casanova S., *Mon. Not. R. Astron. Soc.*, **396-3** (2009) 1629.
[68] Abdo A. *et al.*, *Astroph. J. Lett.*, **706** (2009) L1.
[69] Aharonian F. *et al.*, *Astron. Asrtophys.*, **490-2** (2008) 685.
[70] Villante F. L. and Vissani F., *Phys. Rev. D*, **76** (2007) 125019.
[71] Villante F. L. and Vissani F., *Phys. Rev. D*, **78-10** (2008) 103007.
[72] Morlino G., Blasi P. and Amatoo E., *Astropart. Phys.*, **31-5** (2009) 376.
[73] Berezhko E. G. and Volk H. J., *Astron. Asrtophys.*, **492-3** (2008) 695.
[74] Berezhko E. G., Pühlofer and Volk H. J., *Astron. Asrtophys.*, **505-2** (2009) 641.
[75] Mirabel I. F. and Rodriguez L. F., *Nature*, **392** (1998) 673.
[76] Mirabel I. F., *Science*, **312** (2006) 1759.
[77] Szostek A. *et al.*, *Proc. 31st ICRC, Lodz, Poland* (2009), arXiv:0907.3034.
[78] Albert J. *et al.*, *Science*, **312** (2006) 1771.
[79] Reynoso H. R. and Christiansen G. E., *Astropart. Phys.*, **28-6** (2008) 565.
[80] de Naurios M. *et al.*, *Proc. 29th ICRC, Pune, India*, **4** (2005) 101.104.
[81] Jogler T. *et al.*, *Proc. 31st ICRC, Lodz, Poland* (2009), arXiv:0907.0992.
[82] Aharonian F. *et al.*, *Astron. Asrtophys.*, **460-3** (2006) 743.
[83] Sidro N. *et al.*, *PoS(MQW6)*, (2006) 8.
[84] Vila G. S. and Romero G. E., *AIP Conf. Proc.*, **1085** (2008) 289.
[85] Bordas P., Bosch-Ramon V., Paredes J. M. and Perucho M., *PoS(MQW7)*, **044** (2008) arXiv:0903.3293.
[86] Levinson A. and Waxman E., *Phys. Rev. Lett.*, **87** (2001) 171101.
[87] Distefano C. *et al.*, *Astrophys. J.*, **575** (2002) 378.
[88] Romero G. E. *et al.*, *Astrophys. J.*, **632** (2005) 1093.
[89] Aharonian F. *et al.*, *J. Phys. Conf. Ser.*, **39** (2006) 408.
[90] Aharonian F. *et al.*, *Nature*, **439-1** (2006) 1038.
[91] Kosack K. *et al.*, *Astrophys. J.*, **608** (2004) L97.
[92] Tsuchiya K. *et al.*, *Astrophys. J.*, **606** (2004) L115.
[93] Albert J. *et al.*, *Astrophys. J.*, **638** (2006) L101.
[94] Aharonian F. *et al.*, *Astron. Asrtophys.*, **503-3** (2009) 817.
[95] van Eldik C. *et al.*, *AIP Conf. Proc.*, **1085** (2008) 146.
[96] Eckart A. *et al.*, *J. Phys. Conf. Ser.*, **131-3** (2008) 012002.
[97] Crocker R. M. *et al.*, *Astrophys. J.*, **644** (2007) L95.
[98] Wang Q. D. *et al.*, *Mon. Not. R. Astron. Soc.*, **367-3** (2006) 937.
[99] Aharonian F. *et al.*, *Phys. Rev. Lett.*, **97** (2006) 221102.
[100] Liu S. *et al.*, *Astrophys. J.*, **636** (2006) 798.
[101] Ballantyne D. R. *et al.*, *Astrophys. J.*, **657-1** (2007) L13.
[102] Yusef-Zadhe F. *et al.*, *Astrophys. J.*, **682-1** (2008) 361.
[103] Atoyan A. and Dermer C., *Astrophys. J.*, **617** (2004) L123.
[104] Robert J. Gould and Gerald Schréder, *Phys. Rev. Lett.*, **16** (1966) 252.
[105] Aharonian F. *et al.*, *Nature*, **440** (2006) 1018.
[106] Becker J. K., *Rep. Prog. Phys.*, **458** (2008) 173.
[107] Waxman E. and Bachall J., *Phys. Rev. D*, **59** (1999) 023002.
[108] Battacharije P. and Sigl G., *Phys. Rep.*, **327** (2000) 109.
[109] Fanaroff B., Bernard L. and Riley J. M. , *Mon. Not. R. Astron. Soc.*, **167** (1974) 31.
[110] The MAGIC Collaboration, *Science*, **325** (2008) 1752.
[111] Teshima M. for the MAGIC Collaboration, *Proc. 30th ICRC, Merida, Mexico* (2007).

[112] Mannhein K., *Astrophys. Phys.*, **3** (1995) 295.
[113] Osterbrock D. E., *Rep. Prog. Phys.*, **54** (1991) 579.
[114] Torres D. F. and Anchordoqui L. A., *Rep. Prog. Phys.*, **67** (2004) 1663.
[115] Stecker F. W. *et al.*, *Phys. Rev. Lett.*, **66** (1991) 2697; **59** (1999) 023002.
[116] Achterberg A. *et al.*, *Proc. 29th ICRC, Pune, India* (2005); *Phys. Rev. D*, **76** (2007) 042008.
[117] Stecker F. W. *et al.*, *Phys. Rev. D*, **72** (2005) 107301.
[118] Aharonian F. *et al.*, *Astrophys. J. Lett.*, **695-1** (2009) L40.
[119] VERITAS, VLBA, HESS and MAGIC Collaborations, *Science*, **320** (2009) 444.
[120] Meszaros P., *Rep. Prog. Phys.*, **69** (2006) 2259.
[121] Conner J. P, Evans W. D. and Bellan R. D., *Astrophys. J.*, **157** (1969) L157.
[122] van Paradijs *et al.*, *Nature*, **386** (1997) 686.
[123] Barraud *et al.*, *Astron. Asrtophys.*, **400** (2003) 1021.
[124] Hjorth J. *et al.*, *Nature*, **423-6942** (2003) 847.
[125] Meszaros P., *Nature*, **423-6942** (2003) 809.
[126] Sakamoto T. *et al.*, *Astrophys. J. Suppl.*, **175** (2009) 179.
[127] Band D. L. *et al.*, *Astrophys. J.*, **701-2** (2009) 1673.
[128] Waxman E., *Phys. Rev. Lett.*, **75** (1995) 386.
[129] Guetta D. and Granot J., *Astrophys. J.*, **585** (2003) 885.
[130] Kappes A. for the IceCube Collaboration, *Proc. 31st ICRC, Lodz, Poland* (2009).
[131] Aharonian F. *et al.*, *Astron. Asrtophys.*, **495** (2009) 505.
[132] Albert J. *et al.*, *Astrophys. J.*, **667-1** (2007) 358.
[133] McEnery J. E. for the Milagro Collaboration, *Proc. 31st ICRC, Lodz, Poland* (2009).
[134] Loeb A. and Waxman E., *JCAP*, **0605** (2006) 003.
[135] Benbow W. *et al.*, *Proc. 31st ICRC, Lodz, Poland* (2009).
[136] The Veritas Collaboration, *Nature Lett.*, (2009) doi:10.1038/nature08557.
[137] Acero S. *et al.*, *Science*, **326-5956** (2009) 1080.
[138] Berezinsky V. S. and Zatsepin G. T., *Phys. Lett. B*, **28** (1969) 423.
[139] Protheroe R. J. and Johnson P. A., *Astropart. Phys.*, **4** (1996) 253.
[140] Kalashev O. E. *et al.*, *Phys. Rev. D*, **66** (2002) 063004.
[141] Taylor A. M. and Aharonian F., *Phys. Rev. D*, **76-8** (2009) 083010.
[142] Anchordoqui A. *et al.*, *Phys. Rev. D*, **76** (2007) 123008.
[143] Li Z. and Waxman E., arXiv:0711.4969.
[144] Gaisser T. K., Halzen F. and Stanev T., *Phys. Rep. D*, **258** (1995) 173.
[145] Okun L., *Leptons and quarks* (North Holland, Amsterdam) 1982.
[146] Gandhi R. *et al.*, *Phys. Rev. D*, **58** (1998) 93009.
[147] Dziewonski A., *Earth Sructure in The Encyclopedia of Solid Earth Geography* (Van Nosrtand Reinhold, New York) 1989.
[148] Markov M. A. and Zheleznykh I. M., *Nucl. Phys.*, **27** (1961) 385.
[149] Askaryan G. A., *JETP*, **14** (1962) 441.
[150] Askaryan G. A., *JETP*, **21** (1965) 658.
[151] Askaryan G. A. *et al.*, *Nucl. Instrum. Methods*, **164** (1979) 267.
[152] Fargion D. *et al.*, *Astrophys. J.*, **613** (2004) 1285.
[153] Mobley C. D., *Light and Water: radiative transfer in natural waters* (Academic Press, San Diego) 1994.
[154] Ackermann M. *et al.*, *J. Geophys. Res.*, **111** (2006) D13203.
[155] Bagley P. *et al.*, *Conceptual Design Report for a Deep-Sea Research Infrastructure Incorporating a Very Large Volume Neutrino Telescope in the Mediterranean Sea* (2008) `http://www.km3net.org/CDR/CDR-KM3NeT.pdf`.
[156] Honda M. *et al.*, *Phys. Rev. D*, **75** (2007) 043006.
[157] Ambrosio M. *et al.*, *Astropart. Phys.*, **20-2** (2003) 145.
[158] Wang Y. *et al.*, *Nucl. Phys. B Proc. Suppl.*, **175-176** (2008) 551.
[159] Gladston L. for the IceCube Collaboration, *Proc. 31st ICRC, Lodz, Poland* (2009).
[160] Roberts A. *et al.*, *Rev. Mod. Phys.*, **64** (1992) 259.

[161] Wischnewski R. for the Baikal Collaboration, *Int. J. Mod. Phys. A*, **20** (2005) 6932.
[162] Ayutdinov V. for the Baikal Collaboration, *Nucl. Instrum. Methods A*, **602** (2009) 14.
[163] Andres E. *et al.*, *Astropart. Phys.*, **13** (2000) 1.
[164] Ahrens J. *et al.*, *Phys. Rev. Lett.*, **90** (2003) 251101.
[165] Ahrens J. *et al.*, *Phys. Rev. Lett.*, **92** (2004) 071102.
[166] The IceCube Collaboration, *Phys. Rev. D*, **79** (2009) 102005.
[167] Schukraft A. for the IceCube Collaboration, *Proc. 31st ICRC, Lodz, Poland* (2009).
[168] Gonzalez-Garcia M. C. *et al.*, *JHEP*, **0610** (2006) 075.
[169] Barr G. D. *et al.*, *Phys. Rev. D*, **70** (2004) 023006.
[170] Honda M. *et al.*, *Phys. Rev. D*, **75** (2007) 043006.
[171] The IceCube Collaboration, *IceCube Preliminary Design Document*, (2001) `http://www.icecube.wisc.edu/science/publications/pdd/pdd.pdf`.
[172] Stokstad R. G. for the IceCube Collaboration, *Nucl. Phys. B Proc. Suppl.*, **118** (2003) 514.
[173] Wiebuschv C. for the IceCube Collaboration, *Proc. 31st ICRC, Lodz, Poland* (2009).
[174] Gaisser T. K. for the IceCube Collaboration, *Proc. 30th ICRC, Merida, Mexico* (2007), arXiv:0711.0353.
[175] DeYoung T. for the IceCube Collaboration, *Mod. Phys. Lett. A*, **24** (2009) 1543.
[176] Karle A. for the IceCube Collaboration, *Proc. 31st ICRC, Lodz, Poland* (2009).
[177] Abbasi R. for the IceCube Collaboration, *Astrophys. J. Lett.*, **701** (2009) L47.
[178] Resvanis L. K. for the NESTOR Collaboration, *Proceedings of NOVE, Venice - Italy*, 2006.
[179] Stanley D. J. *et al.*, *Nature*, **273** (1978) 110.
[180] Le Pinchon X. *et al.*, *Geolog. Soc., Special Publ.*, **10** (1982) 319.
[181] Anassontis E. G. for the NESTOR Collaboration, *Nucl. Instrum. Methods A*, **479** (2002) 439.
[182] Rapidis P. for the NESTOR Collaboration, *Nucl. Instrum. Methods A*, **602** (2009) 54.
[183] Aggouras G. for the NESTOR Collaboration, *Astropart. Phys.*, **23** (2005) 377.
[184] Montaruli T. for the ANTARES Collaboration, *Int. J. Mod. Phys. A*, **24** (2009) 1656.
[185] Circella M. for the ANTARES Collaboration, *Nucl. Instrum. Methods A*, **602** (2009) 2.
[186] Vallage B. for the ANTARES Collaboration, *Nucl. Phys. B*, **151** (2006) 407.
[187] Heijboer A. for the ANTARES Collaboration, *Proc. 31st ICRC, Lodz, Poland* (2009), arXiv:0908.0816.
[188] Toscano S. for the ANTARES Collaboration, *Proc. 31st ICRC, Lodz, Poland* (2009), arXiv:0908.0864.
[189] Ambrosio M. *et al.*, *Astrophys. J.*, **564** (2001) 1038.
[190] Abe K. *et al.*, *Astrophys. J.*, **652** (2006) 198.
[191] Migneco E. *et al.*, *Nucl. Instrum. Methods A*, **588** (2008) 111.
[192] Riccobene G. *et al.*, *Astropart. phys.*, **27** (2007) 1.
[193] Capone A. *et al.*, *Nucl. Instrum. Methods A*, **602** (2009) 47.
[194] Ameli F. *et al.*, *IEEE Trans. Nucl. Sci.*, **55-1** (2008) 233.
[195] Aiello S. *et al.*, arXiv:0910.1269 (2009).
[196] Katz U. F. *et al.*, *Nucl. Instrum. Methods A*, **602** (2009) 40.
[197] `http://www.km3net.org/CDR/CDR-KM3NeT.pdf`.
[198] Coniglione R. *et al.*, *Nucl. Instrum. Methods A*, **602** (2009) 98.
[199] Sapienza P. *et al.*, *Nucl. Instrum. Methods A*, **602** (2009) 101.
[200] Vannoni G. *et al.*, *Proceedings of VLVnT09 Athens, Greece*, to be published in *Nucl. Instrum. Methods*.
[201] Sapienza P. *et al.*, *Proceedings of VLVnT09 Athens, Greece*, to be published in *Nucl. Instrum. Methods*.

[202] Kopper C. *et al.*, *Proceedings of VLVnT09 Athens, Greece*, to be published in *Nucl. Instrum. Methods*.
[203] Coniglione R. *et al.*, *Proceedings of VLVnT09 Athens, Greece*, to be published in *Nucl. Instrum. Methods*.
[204] Saltzberg D. *et al.*, *Phys. Rev. Lett.*, **86** (2001) 2802.
[205] Gorham P. W. *et al.*, *Phys. Rev. D*, **72-2** (2004) 023002.
[206] Connolly A., *Nucl. Instrum. Methods A*, **595-1** (2008) 260.
[207] Kravchenko I. *et al.*, *Astropart. Phys.*, **19** (2003) 15.
[208] Kravchenko I. *et al.*, arXiv:0705.4491 (2007).
[209] Hogan D. P. *et al.*, *Phys. Rev. D*, **78** (2008) 075031.
[210] Kravchenko I. *et al.*, *AIP Conf. Proc.*, **870** (2006) 212.
[211] Landsman H. *et al.*, *Nucl. Instrum. Methods A*, **604-1** (2009) S70.
[212] Barwick S. W. *et al.*, *Phys. Rev. Lett.*, **96** (2006) 171101.
[213] Gorham P. W. *et al.*, *Astropart. Phys.*, **32** (2009) 10.
[214] Gorham P. W. *et al.*, *Phys. Rev. Lett.*, **103** (2009) 051103.
[215] Allison P. *et al.*, *Nucl. Instrum. Methods A*, **604-1** (2009) S64.
[216] Besson D. Z., *Astropart. Phys.*, **19** (2003) 15.
[217] Dagkemanskii R. D. and Zheleznykh I. M., *Sov. Phys. JETP Lett.*, **50** (1989) 233.
[218] James C. W. *et al.*, *Proc. 30th ICRC, Merida, Mexico* (2008), p. 1503.
[219] Gorham P. W. *et al.*, *Proc. SPIE*, **4858** (2003) 171.
[220] Artemenko I. A. *et al.*, *Proc. 27th ICRC, Hamburg, Germany* (2001).
[221] Ekers R. D. *et al.*, *Nucl. Instrum. Methods A*, **604-1** (2009) S106.
[222] Riccobene G., *J. Phys. Conf. Ser.*, **136** (2008) 022053.
[223] Askaryan G. A., *Atom. Ener.*, **3** (1957) 153.
[224] Landau L. D. and Pomeranchuk I. J., *Dokl. Akad. Nauk. SSSR*, **92** (1953) 535.
[225] Migdal A. B., *Phys. Rev.*, **103** (1956) 1811.
[226] Sulak L. *et al.*, *Nucl. Instrum. Methods*, **161** (1979) 203.
[227] Learned J. G., *Phys. Rev. D*, **19** (1979) 3293.
[228] Urick R. J., *Sound Propagation in the Sea* (Peninsula Publishing) 1982.
[229] Descamps F. *et al.*, *Proc. 31st ICRC, Lodz, Poland* (2009), arXiv:0908.3251.
[230] Niess V. and Bertin V., *Astropart. Phys.*, **28** (2007) 366.
[231] Karg T. *et al.*, *J. Mod. Phys. Int.*, **A1S1** (2006) 212.
[232] Perkin J. *et al.*, *Nucl. Instrum. Methods A*, **604-1S** (2009) S193.
[233] Vandenbroucke J. *et al.*, *Nucl. Instrum. Methods A*, **604-1S** (2009) S164.
[234] Descamps F. *et al.*, *Nucl. Instrum. Methods A*, **604-1S** (2009) S175.
[235] Lethinen N. G. *et al.*, *Astropart. Phys.*, **17** (2002) 279.
[236] Vandenbroucke J. *et al.*, *Astrophys. J.*, **612** (2005) 301.
[237] Kurahashi N. *et al.*, *Nucl. Instrum. Methods A*, **604-1S** (2009) S127.
[238] Lahman R. *et al.*, *Nucl. Instrum. Methods A*, **604-1S** (2009) S158.
[239] Nosengo N., *Nature*, **426** (2009) 560.
[240] Riccobene G. *et al.*, *Nucl. Instrum. Methods A*, **604-1S** (2009) S149.
[241] The P. Auger Collaboration, *Phys. Rev. Lett.*, **100-21** (2008) 211101.
[242] Abbasi R. U. *et al.*, *Astrophys. J.*, **684** (2008) 790.
[243] Martens K. *et al.*, arXiv:0707.4417.
[244] The P. Auger Collaboration, *Proc. 31st ICRC, Lodz, Poland* (2009).